

1 **Comments and responses on “Trends in global tropospheric hydroxyl radical and methane lifetime since**
2 **1850 from AerChemMIP” by David Stevenson et al.**

3
4 We would like to thank the two anonymous referees for their useful and supportive comments. Their comments
5 are repeated below with our responses in red.

6 **Anonymous Referee #1**

7 This paper analyses the OH trend and methane budget in the period 1850-2014. An important conclusion is that
8 global OH was stable in 1850-1980, after which all three models show an increase of roughly 10%. The analysis
9 convincingly shows that emission changes in Near-Term Climate Forcers (NO_x & CO) are responsible for this
10 behaviour.

11 The manuscript is relatively well prepared, but some improvements are needed, e.g. to the figures, referencing,
12 and discussion.

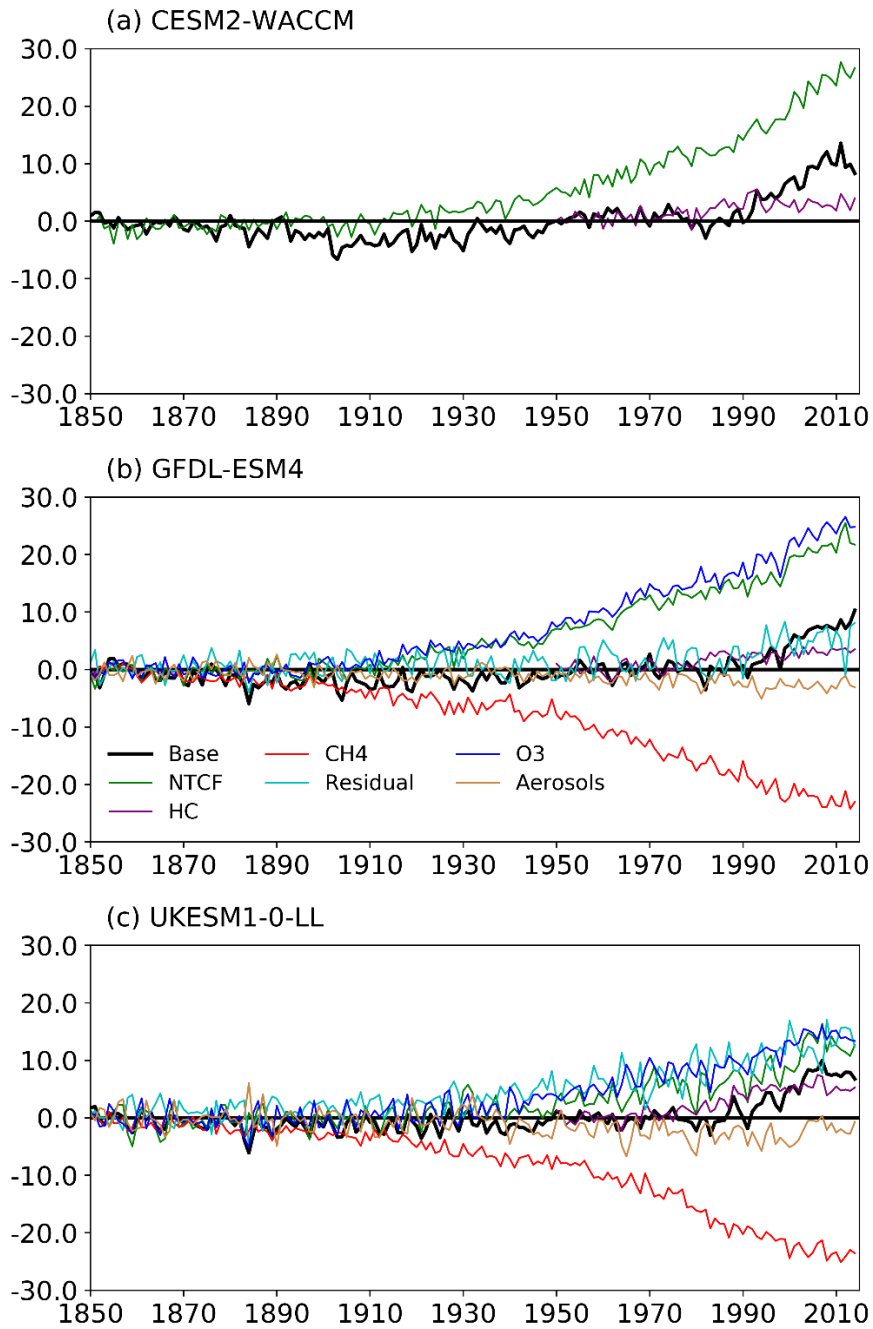
13 Throughout the manuscript authors use “concentration”, while I think in practical calculations, tables, and plots
14 mole fractions are shown. Better to replace concentration by mole fraction.

15
16 We have replaced concentration with mole fraction in all instances except for references to OH, which are
17 concentrations (molecules cm⁻³).

18
19 Concerning the sensitivity simulations: they are sometimes difficult to understand, but I like the calculated impact
20 on the methane mixing ratios.

21 All in all, the paper is concise and to the point, and clearly demonstrates that from a modelling point of view, OH
22 should be increasing. I miss, however, a thorough discussion on the role of climate change on OH (temperature,
23 natural emissions, lighting NO_x.) This is certainly something that needs some more attention, also in light of
24 earlier studies.

25
26 We have now added some more information about climate change. We don't have experiments that specifically
27 isolate climate change impacts on OH. However, the difference between the histSST simulations and the sum of
28 (histSST-piCH₄, histSST-piNTCF and histSST-1950HC) leaves a residual signal that represents the effects of
29 climate change, together with any non-linear interactions between these drivers (see the new Figure 5 below).
30 Assuming these non-linear interactions are negligible, we find that climate change has increased OH, with a
31 similar magnitude to the emissions drivers, and mainly attribute this to increases in water vapour, although other
32 climate change effects may also be important. However, there is evidence that the non-linear interactions are also
33 important, so ascribing the residual term purely to climate change is not possible.



34
 35
 36
 37
 38
 39
 40

Figure 5. The histSST (Base, in black) tropospheric OH anomaly (% change relative to PI) for each year (see Equation 3), for the three models (a) CESM2-WACCM; (b) GFDL-ESM4; and (c) UKESM1-0-LL. The coloured lines represent the contributions to this OH anomaly due to changes since 1850 in CH₄ mole fraction, NTCF emissions, halocarbon mole fraction, O₃ precursor emissions, and aerosols (see Equations 4-8; NB only NTCF and HC experiments from CESM2-WACCM). The residual curve (see Equation 9) is the extra contribution required after linearly adding the curves for CH₄, NTCF and HC that is needed to reproduce the Base anomaly.

41 What also clearly misses is some validation of the model results. I understand that the individual models are (or
42 will be) published, but to gain some confidence in the results, it would be nice to see how e.g. trends in CO are
43 reproduced.

44

45 We have referred to some of the other AerChemMIP studies and other relevant papers.

46

47 Minor comments:

48 R4: wrong. H₂O instead of HO₂.

49

50 Thank you for pointing out this error. We fixed it.

51

52 Line 62: a sink → a dominant sink

53

54 Fixed.

55

56 Line 67: Wrongly suggests that ozone reacts directly with H₂O

57

58 Adjusted text to clarify it is O(¹D) that reacts with H₂O.

59

60 Line 94: GFDL-ESM4 is later called GFDL-AM4, please be consistent.

61

62 We apologise for inconsistencies in naming in the submitted paper. We have revised to consistently use the model
63 names: CESM2-WACCM; GFDL-ESM4; and UKESM1-0-LL, based on the Earth System Grid Federation
64 (ESGF) file names.

65

66 Line 187: Referencing: I miss references to some recent satellite assimilation work which is relevant, e.g.
67 <https://www.atmos-chem-phys.net/15/8315/2015/acp-15-8315-2015.pdf>

68

69 Thank-you for this and the other Miyazaki et al. papers. We have included discussion of these papers (see below).

70

71 Figure 1: I It would be nice to show also the modelled natural NMVOC emissions and how they changed due to
72 climate change and variability in the different models.

73

74 Griffiths et al. (2020) Figure 1 has BVOC emissions. We refer readers to this study, also in the AerChemMIP
75 Special Issue.

76

77 Figure 2: inset: why is the GFDL-ESM4 simulation not included?

78

79 This was a mistake. It is now included.

80

81 Figure 3: The use of the vertical coordinate “model level” is not acceptable.

82

83 We have converted Figures 3 and 4 to now use pressure as the vertical co-ordinate.

84

85 Line 214: It would be nice to compare and discuss these new estimates to existing estimates. Methane is forced
86 to observations, so the lifetime may be biased due to model biases.

87

88 We now compare CH₄ lifetime estimates to existing estimates – values from our models fall within the
89 IPCC(2013) range:

90 *“The multi-model mean whole atmosphere PD chemical lifetime in histSST is 8.4 ± 0.3 yr, lower than the mean
91 PI lifetime of 9.5 ± 0.5 yr (lifetimes for individual models are given in Table 3; the ranges are the standard
92 deviations across the models). These values compare to a whole atmosphere methane lifetime for 2010 (mean \pm
93 1 standard deviation) of 9.1 ± 0.9 yr (Prather et al., 2012), as used by IPCC (Myhre et al., 2013).”*

94 We do not believe that the AerChemMIP experimental set-up, where methane is forced to evolve following
95 observations, introduces any significant model biases.

96

97 Line 251: I do not see why the values of f are unreliable due to changes in halocarbon mole fractions.

98

99 Our method for calculating the methane-OH feedback factor, f, differs from the ‘standard’ method, which would
100 normally use dedicated sensitivity experiments, with a simple +20% perturbation to prescribed methane mole
101 fractions (e.g., Prather et al., 1996, 2001). We use the histSST_piNTCF simulations, which hold NTCFs at pre-
102 industrial levels, but allow methane to increase. These simulations are not ideal, as they also have climate (i.e.,
103 temperature, water vapour, clouds, etc.) changing. From the 1950s onwards, these simulations also allow
104 halocarbons to increase. Elsewhere in the paper, we show that increasing halocarbon levels, and in particular the
105 associated stratospheric ozone depletion, has an impact on OH. For the diagnosis of f we need runs that only
106 perturb methane. Hence we think that when halocarbons also change, the values of f should be considered
107 unreliable. Figure 7 suggests that the effect on f is probably quite small; nevertheless we think it is sensible to just
108 use values of f for the time period 1930-1960 to exclude the later time period when halocarbons (and climate)
109 show larger changes.

110

111 Line 300: Read papers of Miyazaki et al.

112

113 In the revised version we now refer to:

114

115 Miyazaki, K., Eskes, H. J., and Sudo, K.: A tropospheric chemistry reanalysis for the years 2005–2012 based on
116 an assimilation of OMI, MLS, TES, and MOPITT satellite data, *Atmos. Chem. Phys.*, 15, 8315–8348,
117 <https://doi.org/10.5194/acp-15-8315-2015>, 2015

118 Miyazaki, K., Eskes, H., Sudo, K., Boersma, K. F., Bowman, K., and Kanaya, Y.: Decadal changes in global
119 surface NO_x emissions from multi-constituent satellite data assimilation, *Atmos. Chem. Phys.*, 17, 807–837,
120 <https://doi.org/10.5194/acp-17-807-2017>, 2017.

121 Miyazaki, K. and Bowman, K.: Evaluation of ACCMIP ozone simulations and ozonesonde sampling biases using
122 a satellite-based multi-constituent chemical reanalysis, *Atmos. Chem. Phys.*, 17, 8285–8312,
123 <https://doi.org/10.5194/acp-17-8285-2017>, 2017.

124

125 Miyazaki et al. (2015, 2017) and Miyazaki and Bowman (2017) showed that assimilation of O₃, CO and NO₂
126 satellite data into a 3-D Chemistry-Transport Model (CTM) improved the simulated NH/SH ratio of OH from
127 1.26 to 1.18 (cf. an observed ratio of 0.97 ± 0.12 , Patra et al., 2014). These studies clearly show that global OH is
128 sensitive to assimilation of O₃, CO and NO₂ data, due to the strong coupling between the atmospheric chemistry
129 of these species.

130 **Anonymous Referee #2**

131 **1 Overview:**

132 Review of “Trends in global tropospheric hydroxyl radical and methane lifetime since 1850 from AerChemMIP”
133 by Stevenson et al.

134 I apologize for the delay in my review. Stevenson et al. present an analysis of changes in OH abundance and
135 methane lifetime from 1850 to present using simulations from a model intercomparison (CMIP6/AerChemMIP).
136 Specifically, they use output from 3 models: GFDL-ESM4, CESM2-WACCM, and UKESM1. The three models
137 simulate stable OH concentrations prior to 1980 and an increase post 1980. The work then uses a set of sensitivity
138 simulations to diagnose the processes that control the time evolution of OH. Overall, I think the work is both
139 useful and interesting. My main comments relate to the presentation of the interpretation. Specifically, the
140 discussion regarding conflicts with observational MCF constraints and the brevity of the final discussion (there’s
141 only half a page of discussion after laying a solid groundwork in the methods). I feel like this could be expanded
142 to make the work more useful to others. I would suggest minor revisions for the work.

143 **2 Comments:**

144 **2.1 Discussion of MCF constraints**

145 The authors seem to be arguing that these model-derived forward simulations of OH are more reliable than
146 reconstructions.

147

148 *It was not our intention to present the results this way, and we don’t think the model results are more reliable than
149 the reconstructions. We attempted to present the model results and give the OH reconstructions as context, in
150 order to facilitate comparison. We now include uncertainties in the reconstructions from Rigby et al. (2017), which
151 help clarify this comparison.*

152

153 I’d be wary of framing it this way as this paper has ZERO observational constraints.

154

155 This is not quite true – global mean surface methane concentrations are prescribed to evolve following observed
156 levels. Hence the calculated OH values in our paper are consistent with the evolution of observed global mean
157 methane.

158

159 On their face, the results differ from observationally constrained OH estimates and this is the interpretation from
160 the authors (Line 3 in the abstract); however, I'm not convinced they really differ. If the authors were to include
161 the uncertainty estimates from the Rigby et al. (2017) paper, for example, they would likely find that it bounds
162 their results (the uncertainties are included in the supplemental data from the Rigby paper). So I think some of the
163 “disagreement” they see is within the uncertainties.

164

165 We broadly agree with this (see details below).

166

167 Additionally, the OH changes here do seem to agree quite well with the results from Turner et al. (2017) up until
168 2005. One could argue there is a divergence post-2005, but the authors don't really seem to discuss this at all.

169 The authors seem to argue that the entire post-1980 rise differs from the MCF-derived estimates. This is curious
170 to me.

171 I feel that line 3 of the abstract (“The model-derived OH trend since 1980 differs from trends found in several
172 studies that infer OH from inversions of methyl chloroform measurements; however, these inversions are poorly
173 constrained and contain large uncertainties that do not rule out the possibility of recent positive OH trends.”) and
174 some of the main text discussion of the MCF reconstructions needs to be rephrased.

175

176 See below – we now have included the uncertainty estimates from Rigby et al. (2017) into a revised Figure 2 and
177 will adjust the text accordingly. We agree with the reviewer that the AerChemMIP modelled OH trends are (just
178 about) within the uncertainty range derived by Rigby et al. (2017).

179

180 The authors seem to have missed two important papers from Joe McNorton as well:

181 McNorton et al. (2016; <https://doi.org/10.5194/acp-16-7943-2016>) and McNorton et al. (2018;
182 <https://doi.org/10.5194/acp-18-18149-2018>).

183 There are two other recent papers that should also be referenced and briefly discussed:

184 He et al. (2020; <https://doi.org/10.5194/acp-20-805-2020>) and Nguyen et al. (2020;
185 <https://doi.org/10.1029/2019GL085706>). He et al. (2020) also used the GFDL model to simulate methane from
186 1980 to present and find a similar time evolution of OH.

187 Nguyen et al. (2020) look at the impact of chemical cycling on methane and OH.

188

189 These papers are all very relevant and we have incorporated discussion of them into the revised text. McNorton
190 et al. (2016) performed inverse modelling using a 3-D Chemistry-Transport Model (CTM) constrained by MCF
191 data, and found that OH increases contributed significantly to the slowdown in the CH₄ growth rate between 1999
192 and 2006, and that the post-2007 increases in CH₄ growth rate were poorly simulated if OH variations were
193 ignored. McNorton et al. (2018) extended this work with further constraints from GOSAT CH₄ and δ¹³CH₄ and
194 found that the post-2007 CH₄ growth rate surge was most likely due to a combination of a decrease (-1.8 ± 0.4 %)

195 in global OH and increases in CH₄ emissions, although an alternative inversion that assumed fixed OH indicated
196 slightly larger increases in CH₄ emissions. He et al. (2020) used the GFDL-AM4 model, which is the atmospheric
197 component of the GFDL-ESM4 used in this study, and found an upward trend in global OH since 1980 similar in
198 magnitude to our results. Like Gaubert et al. (2017), Nguyen et al. (2020) found that decreasing global CO
199 concentrations since the 2000s have important influences on CH₄ flux inversion results, because of the strong
200 chemical coupling between CO, CH₄ and OH.

201 Collectively, all these earlier studies that have attempted to interpret the observed trends in methane and related
202 species find that OH is sensitive to CO, NO₂, O₃, as well as CH₄. These studies have spanned box models to
203 sophisticated 3-D CTMs, and all appear to be under-constrained in deriving trends in OH. To date, studies have
204 used subsets of the available observational data (e.g., one or more of MCF, CH₄, δ¹³CH₄, CO, ¹⁴CO, NO₂, and
205 O₃), but not yet all available relevant data. The OH trends presented in this study are from state-of-the-art Earth
206 System Models driven by up-to-date emissions estimates from CMIP6, and are consistent with observed trends in
207 CH₄, however other species (e.g., CO, O₃ and NO₂) are allowed to freely evolve. It is unclear if the OH trends
208 simulated by these CMIP6 models are realistic, however, it is clear that the way these models simulate OH is very
209 important for projecting future trends (and understanding past trends) in CH₄.

210

211 **2.2 Processes controlling the OH changes**

212 It would be nice if the authors had one additional schematic type figure that summarizes their findings. There are
213 quite a few acronyms and competing effects that make it confusing at times. Naik et al. (2013) paper had some
214 nice bar charts showing the relative contribution of different factors to the PI-PD OH changes. This really helped
215 follow the argument and understand what the different scenarios are doing. It seems like this would be particularly
216 helpful to the casual reader.

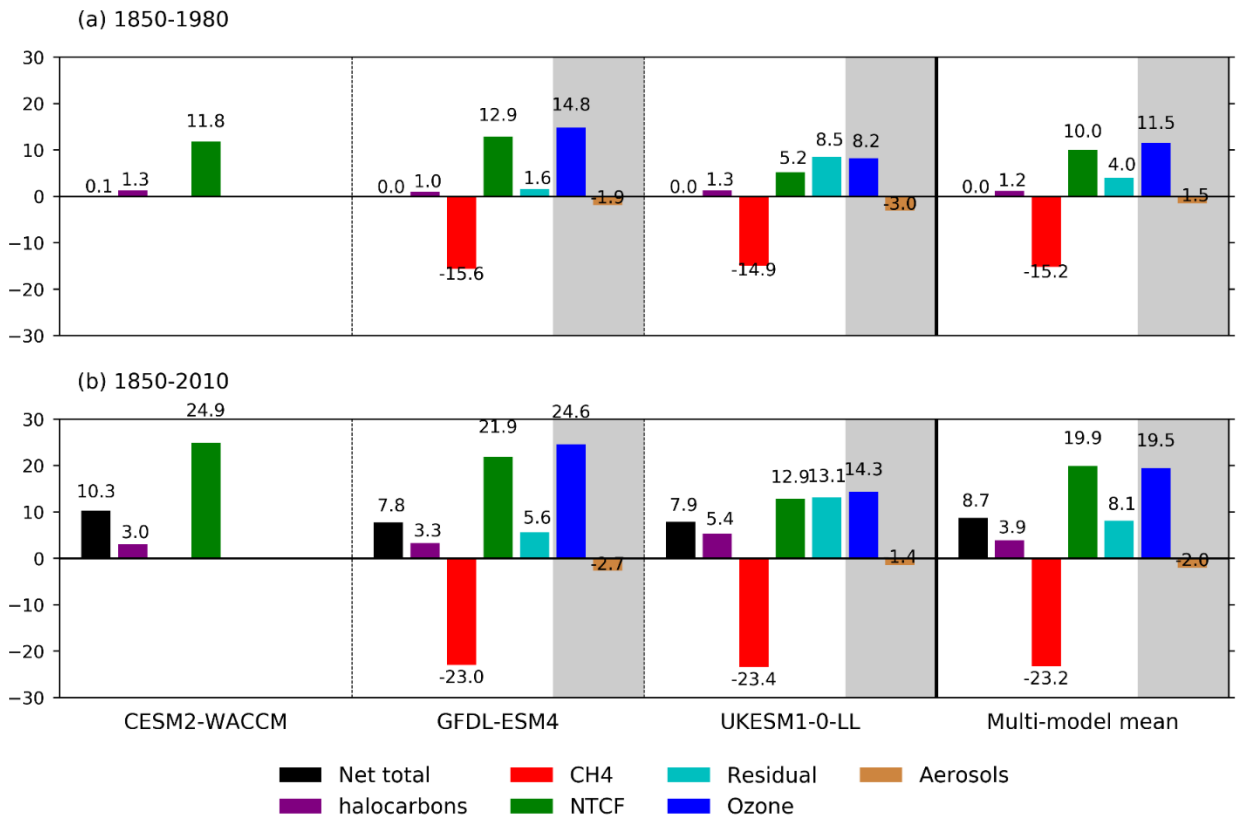
217 As it stands, Figures 5 and 6 are the ones that diagnose the processes controlling the long-term OH changes in the
218 model. But I can imagine many readers having a difficult time figuring out what they are supposed to take away
219 from those figures. As it stands, they are an acronym soup.

220 Personally, I feel that the manuscript would greatly benefit from a final synthesis figure that summarizes the
221 changes described in the abstract and a few additional paragraphs in the discussion section describing this.

222

223

224 We have constructed a new figure (Figure 6) that summarizes the drivers of OH changes – this also includes a
 225 residual term, reflects a combination of climate change effects and non-linear interactions between drivers:
 226



227
 228 **Figure 6. Summary of drivers of OH changes (%), relative to 1850, for the three models and their multi-model mean**
 229 **over: (a) 1850-1980; and (b) 1850-2010. (NB we have used decadal means: 1850 refers to (1850-1859); 1980 is (1975-**
 230 **1984); and 2010 is (2005-2014). The shaded areas show the split of the NTCF signal (green) into ozone precursors (blue)**
 231 **and aerosols (brown), where models have performed both the histSST-piNTCF and histSST-piO3 experiments. The**
 232 **residual values (pale blue) are the differences between the total change (black, from the histSST simulations) and the**
 233 **sum of the changes from CH4 (red), NTCF, and halocarbons (purple). We interpret the residual terms as being due**
 234 **to climate change, in addition to any non-linear interactions between forcings.**

235
 236 **3 Specific comments:**

237 Lines 180–185 (Inserted the relevant lines from the discussion paper here)
 238 “Naus et al. (2019) further investigated the inversion methods used by Rigby et al. (2017) and Turner et al. (2017),
 239 confirming that the derivation of OH from MCF and CH4 is a strongly under-constrained problem, and found that
 240 estimated OH trends with a range of different magnitudes and signs are equally valid solutions from the available
 241 data.”
 242 and 280–283
 243 “Naus et al. (2019) found that the uncertainties inherent in inversion of MCF and other proxy measures of OH are
 244 sufficiently large that OH trends derived from them are less constrained than previously thought, and that positive
 245 recent OH trends are compatible with the MCF measurements.”

247 : I'm confused here, I thought the Rigby et al. (2017) and Turner et al. (2017) paper showed that the problem was
248 under-constrained. If I recall, the Turner paper showed they could fit the data without changing OH and that there
249 were a number of valid solutions. It's not clear what the Naus et al. (2019) paper added?

250

251 The Naus et al. (2019) study nicely illustrates the uncertainties discussed and presented in Rigby et al. (2017). We
252 retain discussion of Naus et al. (2019) in the revised paper, whilst acknowledging that Rigby et al. (2017)
253 quantified uncertainties earlier.

254

255 Lines 198–200

256 “The published inferred trends from different inversion methods show a range of different trends, but there is little
257 resemblance to the upwards trends simulated by the models over this time period.”

258 and 277–280

259 “The strong recent increase is at odds with several studies that use MCF and other proxies to reconstruct OH
260 trends (e.g., Figure 2 inset); however, these show a wide range of trends.”

261

262 This is the discussion that I would disagree with. The model results don't seem that different from the model
263 results (especially if you include error bars from Rigby). You might be able to argue differences post-2005, but
264 1980-2005 seem to be in pretty good agreement. The He et al. (2020) paper also looks at this.

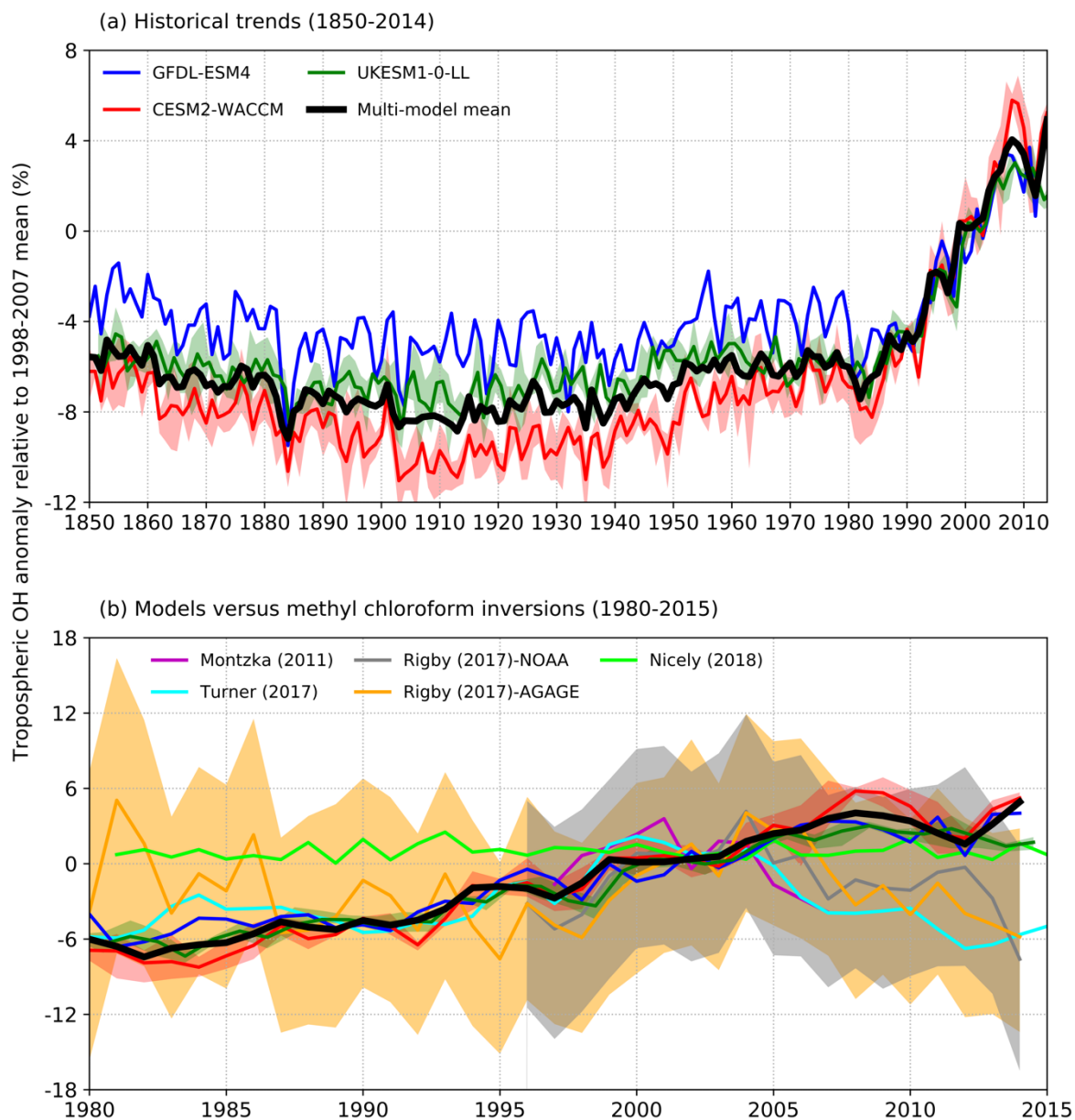
265

266 We have revised this discussion, based on a new version of Figure 2 (below), incorporating uncertainties from
267 Rigby et al (2017).

268

269 The new Figure 2 shows that the AerChemMIP modelled trends are (just about) within the uncertainties of the
270 observation-based estimates of OH. So as the reviewer notes, they are consistent. The model trends do however
271 go from being at the lower end of the uncertainty range in 1980 to the upper edge of the range in 2014. We have
272 adjusted the text and discussion accordingly.

273



274

275 **Figure 2. (a) Time evolution of global annual mean tropospheric OH (1850-2014), expressed as a percentage anomaly**
 276 **relative to the 1998-2007 mean (and ensemble spreads, where available) for GFDL-ESM4 (blue), UKESM1-0-LL**
 277 **(green), and CESM2-WACCM (red), and the multi-model mean (black). (b) Observation-based inversions of global**
 278 **annual mean tropospheric OH for 1980-2015 from Montzka et al. (2011), Rigby et al., 2017, Turner et al., 2017, and**
 279 **Nicely et al. (2018), including ± 1 standard deviation uncertainties for the results from Rigby et al. (2017), with model**
 280 **results from panel (a) overlain.**

Below is a copy of the revised text, highlighting all changes compared to the originally submitted version.

Trends in global tropospheric hydroxyl radical and methane lifetime since 1850 from AerChemMIP

285 David S. Stevenson¹, Alcide Zhao^{1,2,3}, Vaishali Naik²Naik⁴, Fiona M. O'Connor³O'Connor⁵,
Simone Filmes⁴Tilmes⁶, Guang Zeng⁵Zeng⁷, Lee T. Murray⁶Murray⁸, William J.
Collins⁷Collins², Paul Griffiths^{8,9}Griffiths^{9,10}, Sungbo Shim¹⁰Shim¹¹, Larry W.
Horowitz²Horowitz⁴, Lori Sentman²Sentman⁴, Louisa Emmons⁴Emmons⁶

¹School of GeoSciences, The University of Edinburgh, EH9 3FF, United Kingdom

290 ²Geophysical²Department of Meteorology, University of Reading, United Kingdom

³National Centre for Atmospheric Science, University of Reading, United Kingdom

⁴Geophysical Fluid Dynamics Laboratory, National Oceanic and Atmospheric Administration (NOAA), Princeton, NJ08540, USA

⁵Met⁵Met Office Hadley Centre, Exeter, United Kingdom

295 ⁴Atmospheric⁶Atmospheric Chemistry Observations and Modeling Laboratory, National Center for Atmospheric Research, Boulder, CO, USA

⁵National⁷National Institute of Water and Atmospheric Research, Wellington, New Zealand

⁶Department⁸Department of Earth and Environmental Sciences, University of Rochester, Rochester, NY USA

⁷Department of Meteorology, University of Reading, United Kingdom

300 ⁸National⁹National Centre for Atmospheric Science, University of Cambridge, United Kingdom

⁹Department¹⁰Department of Chemistry, University of Cambridge, United Kingdom

¹⁰¹¹ National Institute of Meteorological Sciences, Seogwipo-si, Jeju-do, Korea

Correspondence to: David.S.Stevenson (David.S.Stevenson@ed.ac.uk)

305 **Abstract.** We analyse historical (1850-2014) atmospheric hydroxyl (OH) and methane lifetime data from
CMIP6/AerChemMIP simulations. ~~GlobalTropospheric~~ OH changed little from 1850 up to around 1980, then
increased by around ~~10%,9% up to 2014~~, with an associated reduction in methane lifetime. The model-derived
OH ~~trend since 1980 differs from trends found infrom 1980-2005 are broadly consistent with trends estimated by~~
several studies that infer OH from inversions of methyl chloroform ~~and associated~~ measurements; ~~most inversion~~
310 ~~studies indicate decreases in OH since 2005, however, these inversions are poorly constrained and contain large~~
~~uncertainties that do not rule out the possibility of recent positive OH trends. The recent increases in OH that we~~
~~find are consistent with one previous study that assimilated global satellite derived carbon monoxide (CO) over~~
~~the period 2002-2013 model results fall within observational uncertainty ranges.~~ The upward trend in modelled
OH since 1980 was mainly driven by changes in anthropogenic Near-Term Climate Forcer emissions (increases
315 in anthropogenic nitrogen oxides and decreases in CO). Increases in halocarbon emissions since 1950 have made
a small contribution to the increase in OH, whilst increases in aerosol-related emissions have slightly reduced OH.
Halocarbon emissions have dramatically reduced the stratospheric methane lifetime, by about 15-40%, ~~which has~~
~~been assumed to not change in%;~~ most previous studies. ~~We find that whilst assumed a fixed stratospheric lifetime.~~
~~Whilst~~ the main driver of atmospheric methane increases since 1850 is emissions of methane itself, increased
320 ozone precursor emissions have significantly modulated (in general reduced) methane trends. Halocarbon and
aerosol emissions are found to have relatively small contributions to methane trends. ~~All these factors, together~~
~~with changes and variations of climate and climate driven natural emissions, need to be included~~ ~~These~~
~~experiments do not isolate the effects of climate change on OH and methane evolution, however we calculate~~
~~residual terms that are due to the combined effects of climate change and non-linear interactions between drivers.~~
325 ~~These residual terms indicate that non-linear interactions are important and differ between the two methodologies~~

we use for quantifying OH and methane drivers. All these factors need to be considered in order to fully explain OH and methane trends since 1850; these factors will also be important for future trends.

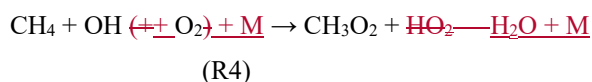
1. Introduction

330 The hydroxyl radical (OH) is a highly reactive, and consequently very short-lived, component of the Earth's atmosphere that lies at the heart of atmospheric chemistry. It is often referred to as the cleansing agent of the atmosphere, as it is the main oxidant of many important trace gases, including methane (CH₄), carbon monoxide (CO), and non-methane volatile organic compounds (NMVOCs). Hydroxyl controls the removal rates of these species, and hence their atmospheric residence times (e.g., Holmes et al., 2013; Turner et al., 2019). Because of this key role in determining the trace gas composition of the atmosphere, it is important to understand what 335 controls OH's global distribution, its temporal evolution, and drivers of changes (e.g., Lawrence et al., 2001; Murray et al., 2014; Nicely et al., 2019).

The primary source of OH is from the reaction of excited oxygen atoms (O(¹D)) with water vapour; the excited oxygen originates from the photolysis of ozone (O₃) by ultra-violet (UV; wavelength < 330 nm) radiation:



345 There is rapid cycling between OH and the hydroperoxyl radical (HO₂) and other peroxy radicals (RO₂, e.g., CH₃O₂). For example, oxidation of CO and CH₄ (and other NMVOCs) consumes OH and generates HO₂ and RO₂:



350 Nitrogen oxides (NO and NO₂, collectively NO_x) tend to push the OH/HO₂ ratio in the other direction, through the reaction:



355 However, in strongly polluted air, NO₂ becomes a dominant sink for OH, through formation of nitric acid (HNO₃). Comprehensive descriptions of hydroxyl radical chemistry are given by, e.g., Derwent (1996), Stone et al. (2012) and Lelieveld et al. (2016).

360 Levels of OH are thus influenced by ambient levels of these other species – in particular, higher concentrations of more CH₄, CO, and NMVOCs will reduce OH, whilst higher concentrations of more NO_x and H₂O will increase OH through ozone chemical production and the subsequent reaction of O(¹D) with H₂O (R2) to produce OH; although the relative influence of different species. Water vapour is incompletely understood (e.g., Wilda key link between physical climate and OH, but there are many others (Isaksen et al., 20192009). For example, many emissions (including biogenic and anthropogenic VOCs, and lightning NO_x), and chemical reactions (e.g., R4)

depend on temperature and other climate variables. Photolysis rates affect OH (e.g., R1) – hence changes in clouds and stratospheric ozone also influence OH.

The global distribution and budget of OH has been estimated by models (e.g., Spivakovsky et al., 1990; Lelieveld et al., 2016). As part of the Fifth Coupled Model Intercomparison Project (CMIP5), the Atmospheric Chemistry and Climate Model Intercomparison Project (ACCMIP) analysed past and future trends in simulated OH (Naik et al., 2013; Voulgarakis et al. 2013) and attributed past changes in methane to changes in anthropogenic emissions of NO_x, CH₄, CO and NMVOCs (Stevenson et al., 2013). However, the relative influences of different processes in driving changes in global OH remains incompletely understood (e.g., Wild et al., 2019).

Evaluation of model-simulated OH requires knowledge of real world OH. In particular, the global distribution of OH is needed to investigate quantities such as methane lifetime. Direct measurement of OH is difficult (Stone et al., 2012). Trends, and distribution estimates of global OH have been derived from can only be inferred indirectly, using measurements of species such as methyl chloroform (Krol and Lelieveld, 2003; Prinn et al., 2005; Montzka et al., 2011; Patra et al., 2014; Rigby et al., 2017), CO (Gaubert et al., 2017) and cosmogenic ¹⁴C (Krol et al., 2008). However, observationally derived global OH levels are uncertain and often show poor agreement with as inputs to inverse models. Discrepancies between, or through assimilation of measurements and of species that constrain OH, such as CH₄, CO and NO₂, into global atmospheric chemistry models are not well understood, although new analyses of. These methods allow trends in global OH over the last few decades to be estimated, with uncertainties (Naus et al., 2019) and new techniques, including Machine Learning (Nicely et al., 2019), are now being applied to the problem. see Section 2.2).

This study presents results from multiple transient 1850-2014 simulations performed for CMIP6 (Eyring et al., 2016) and the associated Aerosol and Chemistry Model Intercomparison Project (AerChemMIP; Collins et al., 2017), and is organised as follows. Section 2 describes how CMIP6 models simulated OH, and methods used in past studies for inferring OH trends from measurements. In Section 3 we present pre-industrial (PI; here taken as the 1850s) and present-day (PD) zonal mean fields of modelled OH and related species, together with historical time-series of global tropospheric OH, and corresponding CH₄ loss rates and lifetimes, including from sensitivity experiments that isolate the effects of specific emissions drivers. Section 4 discusses the results, comparing trends in OH from measurements and models and estimates the roles of specific drivers in the historical evolution of OH. We draw, and draws conclusions in Section 5.

2. Methods

2.1 AerChemMIP CMIP6 experiments and models

We used coupled historical transient (1850-2014) model simulations from CMIP6 (Eyring et al., 2016) and various atmosphere-only historical model simulations from the associated AerChemMIP (Collins et al., 2017). Results from three global state-of-the-art Earth System Models that include detailed tropospheric and stratospheric chemistry were analysed: GFDL-ESM4, CESM2-WACCM, and UKESM1-0-LL (Table 1).

Two base historical transient experiments have been analysed: “historical” and “histSST” (Table 2). The “historical” runs included a fully coupled ocean, and multiple ensemble members. The “histSST” simulations were single member atmosphere-only runs, with monthly mean time-evolving sea-surface temperatures (SSTs) and sea-ice prescribed from one ensemble member of the historical simulations. Identical historical anthropogenic

forcings were applied in all base runs by using prescribed long-lived greenhouse gas and halocarbon concentrationsmole fractions (Meinshausen et al., 2017) and anthropogenic and biomass burning emissions of near-term climate forcers (NTCF; i.e. aerosols and aerosol precursors, and ozone precursors) (van Marle et al., 2017; Hoesly et al., 2018). Emissions of NO_x, CO and NMVOC from 1850-2014 are shown in Figure 1. Natural emissions of these species were either prescribed (e.g., soil NO_x emissions, oceanic CO emissions) or internally calculated (e.g., biogenic isoprene, lightning NO_x) by embedded process-based climate-dependent schemes that differ between models (e.g., ArchibaldGriffiths et al., 2019-2020; Turnock et al., 2020). Methane concentrationsmole fractions were prescribed at the surface based on observations and ice core data (Meinshausen et al., 2017); away from the surface, methane was simulated by the model. However, by prescribing surface concentrationsmole fractions, methane throughout the model domain was effectively prescribed (Figure S1). We also analysed several variants of the histSST base case, with either methane concentrationsmole fractions or emissions of NTCFs fixed at pre-industrial levels, or halocarbon concentrationsmole fractions fixed at 1950 levels. These variants allow us to estimate the roles of different drivers in changing OH (Table 2). For some model variables we separated fields at the tropopause (e.g., to provide a methane lifetime with respect to loss processes in the troposphere and stratosphere as separate values). We used World Meteorological Organisation (WMO) defined tropopause pressures (the AerChemMIP variable ptp) from the models to diagnose this masking. The exact definition used is not critical, as most oxidation occurs well away from the tropopause in the tropical lower atmosphere (cf. tropospheric ozone, where the tropopause definition is much more important; Griffiths et al., submitted2020). Models diagnosed methane loss rates due to chemical destruction in each grid-box – these are dominated by reaction with OH (R4), but also include other reactions, such as the reaction of methane with Cl in the stratosphere. We have used these loss rates to calculate grid-box methane lifetimes. Whole atmosphere chemical lifetimes were calculated by dividing the total methane burden by the total loss flux over the whole model domain (or just the troposphere or stratosphere, for tropospheric and stratospheric lifetimes). We used the histSST-piNTCF simulations to diagnose the methane-OH feedback factor (Prather, 1996). These simulations held NTCF emissions at PI levels, but methane concentrationsmole fractions evolved following its historical trajectory; from 1950 onwards, halocarbon concentrationsmole fractions also increased. The methane-OH feedback is normally diagnosed from dedicated experiments that perturb only the methane concentration,mole fraction (Holmes, 2018), but such experiments are only available for PI conditions within AerChemMIP (e.g., Thornhill et al., submitted2020a). The methane-OH feedback factor, *f*, was calculated as follows:

$$\begin{aligned}
 f &= 1 / (1 - (\ln(\tau_{1930-1960} / \tau_{1850}) / \ln([CH_4]_{1930-1960} / [CH_4]_{1850}))) \quad (1) \\
 f &= \left(1 - \left(\frac{\ln\left(\frac{\tau_{1930-1960}}{\tau_{1850}}\right)}{\ln\left(\frac{[CH_4]_{1930-1960}}{[CH_4]_{1850}}\right)} \right) \right)^{-1} \quad (1),
 \end{aligned}$$

where τ is the total methane lifetime (additionally including a soil sink; CH₄ is taken to have a lifetime with respect to soil uptake of 150-160 yr (Prather, based on results for the 2000s from Spahni et al., 2011, Ito et al., 2012, Kirschke et al., 2013, and Tian et al., 2015, as summarised in Tian et al., 2016; NB here we neglect the tropospheric Cl sink for methane (Allan et al., 2007; Hossaini et al., 2016; Sherwen et al., 2016; Wang et al., 2019; Gromov et

al., 2018; Strode et al., 2020)), $[CH_4]$ is the global mean methane ~~concentration~~mole fraction; both for a particular year(s ~~(or range of years)~~) of the histSST-piNTCF simulation. The reference year is 1850, the first year of the simulation. We took average values between 1930 and 1960 to give the most reliable estimate of f , as this is after a sufficiently large methane perturbation has built up, but before halocarbons interfere with the results in these simulations (see Section 3.3).

We used each model's feedback factor to calculate equilibrium PD methane ~~concentrations~~mole fractions ($[CH_4]_{eq}$) for each sensitivity run, using the diagnosed total methane lifetimes from these experiments. The equilibrium methane ~~concentration~~mole fraction is the methane ~~concentration~~mole fraction that would have been reached if methane ~~concentrations~~mole fractions had not been prescribed in these runs, but rather that methane emissions had been applied, allowing methane ~~concentrations to mole fractions to evolve freely (e.g., Stevenson et al., 2013):~~

~~evolve freely (e.g.,~~

~~$[CH_4]_{eq} = [CH_4]_{ref} (\tau_{PD}/\tau_{ref})^f$ (Fiore et al., 2009; Stevenson et al., 2013):~~

$$[CH_4]_{eq} = [CH_4]_{ref} \left(\frac{\tau_{PD}}{\tau_{ref}} \right)^f \quad (2)$$

where $[CH_4]_{ref}$ is the prescribed methane ~~concentration~~mole fraction in the run, and τ_{ref} is the total methane lifetime in the histSST base experiment, either for PD, or, in the case of histSST-piCH₄, for PI. We illustrate this with two examples: (i) in the histSST_piNTCF case, the equilibrium value is the PD methane ~~concentration~~mole fraction that would have been reached if all NTCF emissions been held at PI levels, whilst CH₄ emissions had followed their historical evolution; and (ii) in the histSST_piCH₄ case, the equilibrium value is the PD methane ~~concentration~~mole fraction that would have been reached ~~is~~ if CH₄ emissions had been held at PI levels, but all other emissions followed their historical evolution. This allows us to clarify modelled influences on CH₄ ~~and OH~~ from specific emissions.

2.2 Inferred OH from measurements

Tropospheric OH has a chemical lifetime of less than a second or so, reflecting its high reactivity, making direct measurement difficult and impractical for constraining global OH distributions (e.g., Stone et al., 2012). Instead, tropospheric mean OH and its variability has traditionally been inferred from measurements of trace gases with lifetimes longer than the timescale of tropospheric mixing and whose primary loss is via reaction with OH. If emissions are well known then observed changes in atmospheric abundance may be related, via inverse methods, to variations in OH. To date, the favoured proxy for estimating OH has been from measurements of methyl chloroform (1,1,1-trichloroethane; CH₃CCl₃; MCF), a synthetic industrial solvent that was banned in the late 1980s as a stratospheric-ozone depleting substance (Lovell, 1977; Singh, 1977; Spivakovsky et al., 1990, 2000; Montzka et al., 2000; Prinn et al., 2001). The inversions have typically spatially represented the global atmosphere as a few boxes.

The earliest MCF inversions predicted relatively large OH variability, reflecting high sensitivity to the uncertainty in residual MCF emissions (Bousquet et al., 2005; Prinn et al., 2005, 2001; Krol and Lelieveld, 2003; Krol et al., 2003). However, Montzka et al. (2011) demonstrated that by the late 1990s, residual emissions had declined

480 sufficiently so as to be a minor source of uncertainty, and that OH varied by at most a few percent in year-to-year
variability. More recently, multi-box models have been used with Bayesian inverse methods to simultaneously
optimize OH and MCF emissions to match MCF observations from the NOAA and the Advanced Global
Atmospheric Gases Experiment (AGAGE) networks, as well as multi-species inversions including methane and
methane isotopologues as additional constraints (Rigby et al., 2017; Turner et al., 2017). Naus et al. (2019) further
investigated the inversion methods used by Rigby et al. (2017) and Turner et al. (2017), confirming that the
485 derivation of OH from MCF and CH₄ is quite poorly constrained and found OH trends with a range of different
magnitudes and signs were consistent with the available data.

The MCF inversions Some inversion studies have used models with greater spatial resolution. McNorton et al.
(2016) performed inverse modelling using a 3-D Chemistry-Transport Model (CTM) constrained by MCF data,
and found that OH increases contributed significantly to the slowdown in the global CH₄ growth rate between
490 1999 and 2006, and that the post-2007 increases in CH₄ growth rate were poorly simulated if OH variations were
ignored. McNorton et al. (2018) extended this work with further constraints from GOSAT CH₄ and δ¹³CH₄ and
found that the post-2007 CH₄ growth rate surge was most likely due to a combination of a decrease (-1.8 ± 0.4 %) in
global OH and increases in CH₄ emissions.

These inversion studies generally find OH to have increased from the late 1980s until the mid-2000s when OH
495 then began to decline (top-left inset of Figure 22b). However, ~~both these recent~~ most inversion studies also found
that ~~optimal~~ solutions exist within the uncertainty of the system when OH was held constant and only emissions
of the reactants were allowed to be optimized. In contrast, Nicely et al. (2018) empirically derived a historic global
mean OH reconstruction by taking a baseline forward OH simulation from the NASA Global Modeling Initiative
(GMI) ~~chemical transport model~~ CTM driven by assimilated meteorology since 1980, and adjusting it based on
500 box-model derived relationships of OH responses to changes in observable parameters such as total ozone
columns from satellites (~~also shown in Figure 2~~). The empirically derived OH reconstruction (also shown in
Figure 2b) was found to be relatively invariant when compared to ~~the other~~ MCF inversions over the past few
decades, which the study suggested reflected chemical buffering of the many competing factors that can influence
OH.

505 Several studies have investigated the constraints imposed on OH by species other than MCF and CH₄. Naus et al.
(2019) further investigated the inversion methods used by Rigby et al. (2017) and Turner et al. (2017), confirming
that the derivation of OH from MCF and CH₄ is a strongly under-constrained problem, and found that estimated
OH trends with a range of different magnitudes and signs are equally valid solutions from the available data.

Gaubert et al. (2017) assimilated time-series of global-scale satellite CO measurements from the Measurement of
510 the Pollution in the Troposphere (MOPITT) project into a global model, and found a decrease in global CO burden
of ~20% over the period 2002-2013. Associated with this decrease in CO was an ~~~8% shortening of the methane
lifetime, and a corresponding increase in OH.~~ 8% shortening of the methane lifetime, and a 7% increase in OH.
Nguyen et al. (2020) also found that decreasing global CO concentrations since the 2000s have important
influences on CH₄ flux inversion results, because of the strong chemical coupling between CO, CH₄ and OH.
515 Assimilation of satellite CO, NO_x and O₃ data (e.g., Miyazaki et al. (2015, 2017), Miyazaki and Bowman, 2017;
Gaubert et al., 2017) demonstrates that OH is sensitive to all these species, and that data assimilation improves
simulation of the hemispheric ratio of OH (Patra et al., 2014).

Collectively, these earlier studies have shown that OH is influenced by CO, NO₂, O₃, as well as CH₄. To date, studies have used subsets of the available observational data (i.e. one or more of MCF, CH₄, δ¹³CH₄, CO, NO₂, and O₃) to constrain OH, but not yet all available relevant data. The OH trends derived from several of these studies, including the uncertainty estimates from Rigby et al. (2017) are summarised in Figure 2b.

3. Results

3.1 Pre-industrial to present-day base simulations

Figure 2a shows time-series (1850-2014) of global annual mean tropospheric OH burden, expressed as a percentage anomaly relative to the 1998-2007 mean value for the three models. This shows typical inter-annual variability in global OH of about ±2-3%, a small decrease (about -3%) in OH from 1850 up to 1910, then a similar magnitude increase up to the 1980s. From the 1980s to 2014, the models show a strong increase in OH of about +10%. All three models show comparable behaviour. Figure S2 compares results between the historical and histSST runs for all models, and finds We find very similar results between the fully coupled (“historical”) and the atmosphere-only (“histSST”) experiments. (not shown). This confirms that it is valid to directly compare and analyse together the results from these two experimental set-ups.

Figure 2b shows several estimates of global tropospheric OH trends over the period 1980-2014 inferred from observations (as described in Section 2.2). The published inferred trends from different inversion methods show a range of different trends, but there is little resemblance to the upwards trends simulated by the models over this time period, including an uncertainty range from Rigby et al. (2017). The inferred trends from different inversion methods show quite a wide range, but are generally upwards from 1980-2005, in broad agreement with the AerChemMIP models. However, from 2005 onwards, the inversions generally indicate downwards trends, whereas the models suggest a continued slight upwards trend. The 1980-2015 model global OH trends are almost always within the ±1 standard deviation uncertainty range from Rigby et al. (2017), although they are close to the lower end of the range in 1980 and just beyond its upper end in 2015.

Figure 3 shows present-day (PD; 2005-2014 decadal mean) zonal mean OH concentrations for the CESM2-WACCM and GFDL-AM4 models. The vertical co-ordinate is model level pressure, and the zonal mean WMO tropopause is indicated. Both All models show high OH values between 30°S and 30°N in the lower to middle troposphere, with larger values in the Northern Hemisphere (NH). Peak OH concentrations occur in the stratosphere, but it is the tropospheric OH that mainly determines the magnitude and distribution of the methane oxidation flux (Figure S3).

Figure 3 also shows changes in OH from pre-industrial (PI; 1850-1859 decadal mean) to PD, expressed as the percentage change relative to PD. This reveals local increases of up to 30% over 50% in zonal mean tropospheric OH, in particular over polluted regions of the NH mid-latitudes, but also a local decrease of up to 15% over 10% in the Southern Hemisphere (SH) mid- to upper-troposphere at around 20°S. The PD-PI figures also show both the PD and PI tropopauses, and indicate insignificant changes in tropopause height over the historical era.

Figure 4 shows the zonal mean distribution of local methane lifetime, which ranges from about 2.5 years in the tropical lower troposphere to >20 years in colder, drier high latitudes and in the vicinity of the tropopause. Short lifetimes also occur in the stratosphere, but do not contribute significantly to the whole atmosphere lifetime due to the low air densities at high altitudes. Whole atmosphere PD (PI) lifetimes in histSST are 8.4 (9.6) yr (CESM2-

WACCM), 8.3 (9.1) yr (UKESM1) and 8.6 (10.0) yr (GFDL-ESM4) (Table 3). Lifetimes have fallen since the PI, reflecting increases in OH. Short

lifetimes also occur higher in the stratosphere, but do not contribute significantly to the whole atmosphere chemical lifetime due to the low air densities at high altitudes. The multi-model mean whole atmosphere PD chemical lifetime in histSST is 8.4 ± 0.3 yr, lower than the mean PI lifetime of 9.5 ± 0.5 yr (lifetimes for individual models are given in Table 3; the ranges are the standard deviations across the models). These values compare to a whole atmosphere methane lifetime for 2010 (mean ± 1 standard deviation) of 9.1 ± 0.9 yr (Prather et al., 2012), as used by IPCC (Myhre et al., 2013). Lifetimes have fallen since the PI, mainly reflecting increases in OH.

3.2 Historical sensitivity simulations

The drivers of these changes in OH and methane lifetime were explored further using a range of results from sensitivity experiments based on the histSST simulations. These kept anthropogenic emissions or concentrations/mole fractions of particular species, or groups of species, at their PI or 1950 levels (Table 2). Figure 3 shows how zonal mean OH in the models responded to fixing NTCF emissions at PI levels and halocarbon concentrations/mole fractions at 1950 levels; Figure S5 shows additional results from the GFDL-AM4 model from the piCH4 and piO3 simulations. The panels in Figures Figure 3 and S5 shows percentage changes in OH relative to the PD histSST base case (corresponding absolute changes in OH are shown in Figure S6). Figure 4 shows percentage changes in methane lifetime (corresponding absolute changes are shown in Figure S8). Figure 5 shows time series of how the annual tropospheric OH burden anomaly evolves in each sensitivity run, whilst Figure 6 shows the equivalent evolution of whole atmosphere methane lifetime. Figure 6 also deconvolves the methane lifetime into its tropospheric and stratospheric components.

We define the annual tropospheric OH burden anomaly in the base histSST simulations at time t ($\Delta OH_{Base}(t)$), as the percentage change in OH since PI (1850-1859):

$$\Delta OH_{Base}(t) = 100\% \times \left(\frac{OH_{histSST}(t) - OH_{histSST}(PI)}{OH_{histSST}(PI)} \right) \quad (3a)$$

or, for clarity, dropping the (t) and substituting OH_{PI} for $OH_{histSST}(PI)$:

$$\Delta OH_{Base} = 100\% \times \left(\frac{OH_{histSST} - OH_{PI}}{OH_{PI}} \right) \quad (3b)$$

We then use each sensitivity run to isolate the contributions to this overall OH anomaly from changes in CH₄ mole fraction, NTCF emissions, halocarbon mole fraction, and O₃ precursor emissions since 1850:

$$\Delta OH_{CH_4} = 100\% \times \left(\frac{OH_{histSST} - OH_{histSST_piCH_4}}{OH_{PI}} \right) \quad (4)$$

$$\Delta OH_{NTCF} = 100\% \times \left(\frac{OH_{histSST} - OH_{histSST_piNTCF}}{OH_{PI}} \right) \quad (5)$$

$$\Delta OH_{HC} = 100\% \times \left(\frac{OH_{histSST} - OH_{histSST_1950HC}}{OH_{PI}} \right) \quad (6)$$

$$\Delta OH_{O_3} = 100\% \times \left(\frac{OH_{histSST} - OH_{histSST_piO_3}}{OH_{PI}} \right) \quad (7)$$

595

Since the ΔOH_{NTCF} and ΔOH_{O_3} anomalies only differ in that the former includes the effects of aerosols, then assuming the impacts of aerosols and O_3 precursors on OH do not interact with each other, we can also isolate the contribution from changes in aerosols to the overall OH anomaly:

$$600 \quad \Delta OH_{aerosol} = \Delta OH_{NTCF} - \Delta OH_{O_3} \quad (8)$$

In addition, we can calculate a ‘residual’ contribution, i.e. the component of the overall OH anomaly that is left after linearly adding all the other components:

$$605 \quad \Delta OH_{residual} = \Delta OH_{Base} - \Delta OH_{CH_4} - \Delta OH_{NTCF} - \Delta OH_{HC} \quad (9)$$

This residual component represents the contribution of climate change to the OH anomaly, along with any contributions from non-linear interactions between components. Non-linearities may arise, for example, because the response of OH to changes in CH_4 is likely to differ depending on whether NTCFs, such as NO_x , are at PI or PD levels. Such interactions are not isolated by our methodology, and it is unclear whether the climate change signal or the effects of non-linearities dominate this residual term.

Figure 5 shows time series of how the base OH anomaly (Equation 3) evolves, together with each of the components (Equations 4-9) that contribute to the base anomaly. Figure 6 compares the magnitudes of these various drivers of OH changes over two time periods: 1850-1980 and 1850-2010. Figure 7 shows the evolution of whole atmosphere methane lifetime for the base histSST runs and each sensitivity run. Figure 7 also separates the methane lifetime into its tropospheric and stratospheric components.

Figures 5 and 6 shows that the evolution of OH has been mainly controlled by the balance between the growth of methane, which has acted to reduce OH by over 20%, and the changes of NTCF emissions (and in UKESM1-0-LL, the residual term), which have tended to increase OH. Because these opposing drivers have similar magnitudes, small mismatches between them are key, and the other minor drivers can also be important contributors to the overall trend in OH.

The impact of increases in NTCF emissions since 1850 up to PD was to generally increase tropospheric OH by 20-30% (Figures 3 and 5) 10-50% in the zonal mean (Figure 3) and 13-22% across the whole troposphere (Figures 5 and 6); this mainly reflects the dominant role of NO_x increases, whose impact overwhelms the impacts of increasing CO (up to ~1990) and NMVOC emissions, which will have tended to reduce OH. Since about 1990, global CO emissions have reduced, (Figure 1), also contributing to the increase in OH. The overall impact of increased/changed emissions of NTCFs has been to reduce the methane lifetime (Figures 4 and 6, Table 3). This is mainly driven by increases in NO_x emissions. The structure seen in the zonal mean PD-PI change in OH (Figure 3, column 2) can be largely explained by the change in NTCF emissions (Figure 3, column 3), with the effects of methane mole fraction increases superimposed. Note that increasing methane also increases CO, and both these reduce OH. We are unable to isolate the effects of CO in our experiments.

630

Emissions of halocarbons since 1950 have led to polar stratospheric ozone depletion, mainly in the SH. This has increased stratospheric OH levels, but also increased tropospheric OH, due to increased penetration of ultra-violet (UV) radiation, and consequently higher photolysis rates (Figure 3). The overall impact on tropospheric OH and methane lifetime is comparatively small (Figures ~~5 and 6~~ 4-7, Table 3), but the impact on methane lifetime in the stratosphere has been dramatic, reducing it from ~170 yr to ~140 yr ~~in (CESM2-WACCM, and)~~, from ~140 yr to ~80 yr ~~in (GFDL-AM4ESM4) and from ~190 yr to 145 yr (UKESM1-0-LL)~~ (Figure 67). These changes are mainly driven through changes in stratospheric Cl. These values can be compared to an assumed constant value for the lifetime of methane with respect to stratospheric chemical destruction of 120(\pm 20%) yr in IPCC-AR5 (Prather et al. 2012).

~~Increases of methane since the PI have reduced OH (Figures 5 and S5), and lengthened the methane lifetime (Figure 6, Table 3). The effects of increased emissions of aerosols and aerosol precursors can be diagnosed by comparing/differencing the piO3 (Figure S5 and 5) and piNTCF simulations. These indicate that aerosols (Equation 8). Aerosols have slightly reduced OH (Figures 5 and 6) and lengthened the methane lifetime, (Figure 7), but the effect is small in magnitude compared to most other effects (Figure . For the two models able to diagnose the residual term, they both suggest a positive impact on OH, although by variable amounts (6)-13%, with a larger residual term in UKESM1-0-LL. We suggest this term may reflect increases in humidity associated with climate change and an increase in the primary OH production flux (Equation R2). However, exactly what the residual terms represent remains uncertain.~~

3.3 Contribution of OH drivers to PI-PD changes in methane

Figure 7 shows values for the methane-OH feedback factor (from a modified version Equation 1, using values for individual years, rather than 1930-1960) calculated for every year in the histSST-piNTCF simulations. In the first few decades, the methane changes are small and the variability of the methane lifetime yields large fluctuations in f. Beyond about 1960, changes in halocarbon ~~concentrationsmole fractions~~ mean that the values of f are unreliable. We therefore use the average value over the time period 1930-1960 as our best estimate of the feedback factor. This yields a value of 1.25 for CESM2-WACCM and 1.23 for GFDL-AM4-CollinsESM4. Thornhill et al. (submitted2020a) find values of f from the piClim simulations of 1.3430 for GFDL-AM4ESM4 and 1.3532 for UKESM1-0-LL. The values derived using equation (1) are probably slightly smaller because the histSST_piNTCF runs also include increases in temperature and humidity. These values are similar to the range of values found in previous studies: 1.23-1.35 (Stevenson et al., 2013; six models); 1.19-1.28 (Voulgarakis et al., 2013; two models, year 2000 conditions); and 1.33-1.45 (Prather et al., 2001; seven models). Using the values of f for 1930-1960 (Figure 7) ~~for CESM2-WACCM and GFDL-ESM4, and the value of 1.32 for UKESM1-0-LL (Thornhill et al., 2020a)~~ and the lifetimes presented in Table 3, we calculate equilibrium PD methane ~~concentrationsmole fractions~~ for all sensitivity experiments (Table 4).

Observed PI and PD methane levels are 808 ppb and 1794 ppb, respectively. Holding NTCFs at PI levels increases PD methane by 16-~~3233~~%. This is more intuitively interpreted in terms of the impact of the increased emissions of NTCFs: they have tended to reduce PD methane by this amount. Similarly, the impact of halocarbon emissions has been to reduce PD methane by ~~107~~-15%.

Taking the average of results from the GFDL ~~model alone, ESM4 and UKESM1-0-LL models (that have values for all categories)~~, holding methane emissions at PI levels would have led to PD methane levels of ~~529516~~ ppbv,

35% (27936% (292 ppbv) lower than PI ~~concentrations~~ mole fractions. Hence the net impact of increasing methane emissions has been to increase methane ~~concentrations~~ mole fractions from 529516 ppbv to 1794 ppbv, an increase of ~~12651278~~ ppbv. ($\Delta[CH_4]_{eqCH_4}$). This increase is 2830% larger than the simple observed PI to PD increase in methane (986 ppbv). ~~$\Delta[CH_4]_{eq_{obs}}$~~ . The net impact of ~~ozone precursor (NO_x + CO + NMVOC)NTCF~~ emissions was to reduce PD methane by ~~657480~~ ppbv. ~~Increases~~ ($\Delta[CH_4]_{eqNTCF}$), whilst increases in halocarbon emissions reduced PD methane by ~~174149~~ ppbv. ~~Increases in aerosol related emissions increased PD methane by 74 ppbv.~~ ($\Delta[CH_4]_{eqHC}$). These diagnosed contributions do not linearly add up to give the observed total, ~~because~~ ~~a~~; there is a residual term, as also found when attributing the OH changes to drivers. Following a similar format to Equation 9, we can diagnose this residual term:

$$\begin{aligned} \Delta[CH_4]_{eq_{residual}} &= \Delta[CH_4]_{eq_{obs}} - \Delta[CH_4]_{eq_{CH_4}} - \Delta[CH_4]_{eq_{NTCF}} - \Delta[CH_4]_{eq_{HC}} \\ &= 986 - 1278 + 480 + 149 = 337 \text{ ppbv} \end{aligned} \quad (10)$$

We tentatively attributed the OH residual term to climate change impacts, as the residual OH increase could physically be linked to water vapour increases. However, the residual change in equilibrium methane is positive, whilst it would be expected to be negative in order to match the positive residual OH term. The other attributions for OH and equilibrium methane are more well-behaved and consistent set of experiments (i.e. where all the terms are added one by one to a base case) has not been performed, and there are significant ~~non-linearities in the system behaviour (i.e., the response to changes linear interactions between drivers are important, and differ in NTCFs depends on the background levels of CH₄, etc.)~~ strength between our attribution methodologies for OH and methane. This means that perfect quantitative attribution cannot be achieved, and attribution of the residual term to climate change effects is rather uncertain. Nevertheless, the magnitudes of these attribution terms are a useful qualitative indicator/indicators of their/the relative importance of different drivers of changes in OH and methane lifetime.

4. Discussion and conclusions

Modelled OH trends presented in this study are from state-of-the-art Earth System Models driven by CMIP6 historical forcings, including observed trends in CH₄ and halocarbon mole fractions. The latter drive stratospheric ozone depletion in the models, which strongly influences tropospheric UV levels and hence photolysis rates. Apart from CH₄, all other reactive species that control OH (e.g., CO, O₃, NO₂ and H₂O) freely evolve in the simulations, in response to prescribed CMIP6 emissions and simulated climate. These model simulations of OH are very important for understanding past trends and projecting future trends in CH₄.

The base model simulations presented here all show similar, consistent historical trends in global OH. They suggest, with relative stability of OH from the PI 1850 up to ~1980, followed by a strong (~10%) increase (9 %) increases up to the present-day (Figures Figure 2 and S2). The earlier stability is in good agreement with previous studies (e.g., Naik et al., 2013). The strong recent increase from 1980 to 2005 is at odds broadly consistent with several studies that use MCF and other proxy species to reconstruct OH trends (e.g., Figure 2 inset); from observations; however, since 2005 most of these reconstructions indicate a decrease in OH, whereas our models indicate a continued increase (Figure 2b). However, these reconstructions show a wide range of trends. Naus, and

our modelled trends fall just about within the uncertainty range estimated by Rigby et al. (2019) found that the uncertainties inherent in inversion of MCF and other proxy measures of OH are sufficiently large that OH trends derived from them are less constrained than previously thought, and that positive recent OH trends (2017). The magnitudes of the model's recent increases are compatible with the MCF measurements. The magnitude of the recent increase concurs with similar to results from Gaubert et al. (2017), who assimilated satellite-derived trends in CO since 2002 into an Earth System Model. Several OH inversions have used multiple observational data-sets (Miyazaki et al., 2015; McNorton et al., 2018), and as the time-series of observations, particularly satellite data, lengthens, uncertainties on real-world OH trends will hopefully reduce, providing stronger constraints for models. Historical We attempted to quantify the component drivers of the changes in OH using a series of idealised model sensitivity experiments. These experiments show exhibit relatively consistent OH responses across the models (Figure Figures 5 and 6), and show that the evolution of methane and ozone precursor emissions have strongly influenced OH trends. Halocarbon and aerosol emissions have had relatively small impacts. related emissions have had relatively small impacts. We also diagnose a residual component that represents the impact of climate change and non-linear interactions between drivers. Other studies have indicated that climate variations and change influence OH (e.g., Naik et al., 2013; Murray et al., 2014; Turner et al., 2018). The modelled increase in OH since 1980 is because the influence of NTCF emissions, together with this residual term, outweighs the effects of increasing CH₄ (Figure 6). These experiments did not separate the effects of different ozone precursors, but these have been explored in previous studies (Stevenson et al., 2013; Holmes et al., 2013), where increases in anthropogenic NO_x emissions have been found to be the main NTCF driver of OH increases. Recent reductions in anthropogenic CO emissions (Figure 1) are clearly also important (Gaubert et al., 2017; Griffiths et al., submitted-2017), but our experiments are unable to separate the relative impacts of these two species.

The trends in OH are associated with trends in methane lifetime (Figure 7), and we have used these to estimate the influence of individual drivers on methane mole fraction, by calculating equilibrium methane levels from the changes in lifetime (Table 4). Drivers that increase OH lead to reductions in methane lifetime and equilibrium methane. The residual component for OH is positive, and may mainly physically represent the rise of water vapour associated with climate warming. This finding is broadly consistent with results presented by Thornhill et al., 2020b) of the negative impacts on methane lifetime found in 4xCO₂ experiments (see their Table 15). However, the residual component we diagnosed from changes in equilibrium methane is also positive, which suggests that non-linear interactions show different impacts in our two methodologies that diagnose residual effects, and that the residual term may not be a good indicator of climate change effects alone. These results indicate that methodologies to isolate drivers of OH and methane changes need careful interpretation, as non-linearities (i.e. couplings between drivers) appear to be important.

Although halocarbon emissions have had quite small effects on the whole atmosphere methane lifetime, they have had dramatic impacts on methane's stratospheric chemistry, where its lifetime may have reduced by up to about 40% between 1960 and 1990 (Figure 67). Previous studies have generally assumed a fixed stratospheric sink lifetime for methane (e.g., Prather et al, 2012).

These findings have implications for future trends in OH and methane (e.g., Holmes et al., 2013), and for how we interpret recent trends (Turner et al., 2019). The relative roles of changing emissions of methane, CO and NO_x all have important competing consequences. Data assimilation of CO trends (Gaubert et al. 2017) has illustrated that this is a major driver of recent OH trends. Our results indicate that similar studies, for example assimilation of

750 ~~NO₂ data, may also uncover important extra information. Other studies have indicated that climate variations and change also influence OH (e.g., Murray et al., 2014; Turner et al., 2018). All these factors need to be included in holistic assessments of OH and methane change.~~

5. Conclusions

755 ~~The CMIP6/AerChemMIP results indicate that global atmospheric OH changed little from 1850 up to around 1980, but subsequently has increased by around 10%. The model derived trend since 1980 differs from trends found in several studies that infer OH from inversions of MCF measurements; however, these are poorly constrained and contain large uncertainties that do not rule out recent positive OH trends. The recent increases in OH that we find are consistent with one study that assimilated global satellite derived CO over the period 2002–2013. Further research is required to better reconcile and quantify model and measurement derived OH trends and their implications. All these factors need to be included in holistic assessments of OH and methane change.~~

760 ~~We find that the major drivers of the recent upward trend in OH seen in the model simulations are increases in anthropogenic NO_x emissions and decreases in anthropogenic CO emissions. Increases in halocarbon emissions have made a small contribution to the increase in OH, whilst increases in aerosol-related emissions have tended to slightly reduce OH. Halocarbon emissions have dramatically reduced the stratospheric methane lifetime, by about 15–40%, and this impact should be accounted for in future studies.~~

765 The CMIP6/AerChemMIP model simulations contain many useful diagnostics that will allow us to better understand the drivers of atmospheric OH and methane trends. This study represents a very preliminary initial analysis of this rich multi-model, multi-experiment dataset.

Code and data availability

770 This work uses simulations from multiple models participating in the AerChemMIP project, as part of the Coupled Model Intercomparison Project (Phase 6; <https://www.wcrp-climate.org/wgcm-cmip>); model-specific information can be found through references listed in Table 1. Model outputs are available on the Earth System Grid Federation website (<https://esgf-data.dkrz.de/search/cmip6-dkrz/>). The model outputs were pre-processed using netCDF Operator (NCO) and Climate Data Operator (CDO). The analysis was carried out using Bash and
775 Python programming languages.

Author contributions

A large team of modellers generated the data used in this study: VN, LWH and LS produced the GFDL model data; FMO, GZ, PG and SS produced the UKESM data; ST and LE produced the CESM data. AZ synthesized and analysed the data and produced the figures. DSS wrote the paper, incorporating comments from all authors.

780 **Acknowledgements**

DSS acknowledges support from the NERC grants NE/N003411/1 and NE/S009019/1, and the ARCHER UK National Supercomputing Service (<http://www.archer.ac.uk>). AZ acknowledges support from a Joint Scholarship from the China Scholarships Council/University of Edinburgh and the UK-China Research and Innovation Partnership Fund through the Met Office Climate Science for Service Partnership (CSSP) China as part of the Newton Fund (grant no. H5438500). GZ was supported by the NZ Government's Strategic Science Investment Fund (SSIF) through the NIWA programme CACV. WC acknowledges funding received from the European Union's Horizon 2020 research and innovation programme under grant agreement No 641816 (CRESCENDO). ST, LE and the CESM project is supported primarily by the National Science Foundation. This material is based upon work supported by the National Center for Atmospheric Research, which is a major facility sponsored by the NSF under Cooperative Agreement No. 1852977. Computing and data storage resources, including the Cheyenne supercomputer (doi:10.5065/D6RX99HX), were provided by the Computational and Information Systems Laboratory (CISL) at NCAR. SS was supported by the Korea Meteorological Administration Research and Development Program "Development and Assessment of IPCC AR6 Climate Change Scenario", grant agreement number 1365003000.

795 **References**

[Allan, W., Struthers, H., and Lowe, D.: Methane carbon isotope effects caused by atomic chlorine in the marine boundary layer: Global model results compared with Southern Hemisphere measurements, *J. Geophys. Res.-Atmos.*, 112, D04306, <https://doi.org/10.1029/2006JD007369>, 2007.](#)

Archibald, A. T., ~~O'Connor~~O'Connor, F. M., ~~N.L.~~Abraham, ~~S.N.L.~~Archer-Nicholls, ~~M.P.S.~~Chipperfield, M. P., ~~Dalvi~~G.A.M., ~~Folberth~~F.G.A., ~~Dennison~~S.S.F., ~~Dhomse~~P.T.S.S., ~~Griffiths~~C.P.T., ~~Hardacre~~A.J.C., ~~Hewitt~~R.A.J., ~~Hill~~C.E.R.S., ~~Johnson~~J.C.E., ~~Keeble~~M.O.J., ~~Köhler~~M.O., ~~Morgenstern~~J.P.O., ~~Mulcahy~~C.J.P., ~~Ordóñez~~R.J.C., ~~Pope~~S.R.J., ~~Rumbold~~M.R.S.T., ~~Russo~~N.M.R., ~~Savage~~A.N.H., ~~Sellar~~M.A., ~~Stringer~~S.M., ~~Turnock~~Θ.S.T., ~~Wild~~O., and ~~G-Zeng~~Zeng, G.: Description and evaluation of the UKCA stratosphere–troposphere chemistry scheme (StratTrop vn 1.0) implemented in UKESM1, *Geosci. Model Dev. Disc.*, 13, 1223–1266, <https://doi.org/10.5194/gmd-2019-246>, 2019–13-1223-2020, 2020.

Bousquet, P., Hauglustaine, D., Peylin, P., Carouge, C. and Ciais, P.: Two decades of OH variability as inferred by an inversion of atmospheric transport and chemistry of methyl chloroform, *Atmos. Chem. Phys.*, 5, 2635–2656, 2005.

Collins, W. J., Lamarque, J.-F., Schulz, M., Boucher, O., Eyring, V., Hegglin, M. I., Maycock, A., Myhre, G., Prather, M., Shindell, D., and Smith, S. J.: AerChemMIP: quantifying the effects of chemistry and aerosols in CMIP6, *Geosci. Model Dev.*, 10, 585-607, doi:10.5194/gmd-10-585-2017, 2017.

Derwent R. G.: The influence of human activities on the distribution of hydroxyl radicals in the troposphere, *Philosophical Transactions of the Royal Society of London. Series A: Mathematical, Physical and Engineering Sciences*, [doi:10.1098/rsta.1996.0018](https://doi.org/10.1098/rsta.1996.0018), 1996.

815 Dunne, J. P., [Horowitz, L. W., Adcroft, A. J., Ginoux, P., Held, I. M., John, J. G., et al.: \(2020\). The GFDL Earth System Model version 4.1 \(GFDL-ESM4-ESM 4.1\): ModelOverall coupled model](#) description and simulation

characteristics. *Journal of Advances in Modeling Earth Systems*, ~~submitted~~, 12, e2019MS002015. [https://doi.org/10.1029/](https://doi.org/10.1029/https://doi.org/10.1029/)

Emmons, L. ~~K.~~, Schwantes, R. H., Orlando, J. J., Tyndall, G., ~~Schwantes, R. H.~~, Kinnison, D. ~~E.~~, Lamarque, J. ~~F.~~, Marsh, D. ~~R.~~, Mills, M. ~~J.~~, Tilmes, ~~S.~~, ~~and Lamarque, J. F.~~: The MOZART ~~Bardeen, C., Buchholz, R. R., Conley, A., Gettelman, A., Garcia, R., Simpson, I., Blake, D. R., Meinardi, S., Pétron, G. (2020), The Chemistry Mechanism in the Community Earth System Model version 2 (CESM2), *J. Advances in review, J. Adv. Modeling Earth Systems*, 2019-12, <https://doi.org/10.1029/2019MS001882>.~~

Eyring, V., Bony, S., Meehl, G. A., Senior, C. A., Stevens, B., Stouffer, R. J., and Taylor, K. E.: Overview of the
 825 Coupled Model Intercomparison Project Phase 6 (CMIP6) experimental design and organization, *Geosci. Model Dev.*, 9, 1937-1958, doi:10.5194/gmd-9-1937-2016, 2016.

Gaubert, B., Worden, H.M., Arellano, A.F.J., et al.: Chemical feedback from decreasing carbon monoxide emissions. *Geophysical Research Letters*, 44, <https://doi.org/10.1002/2017GL074987>, 2017.

Gettelman, A., Mills, M. J., Kinnison, D. E., Garcia, R. R., Smith, A. K., Marsh, D. R., Tilmes, S., Vitt, F.,
 830 Bardeen, C. G., McInerney, J., Liu, H.-L., Solomon, S. C., Polvani, L. M., Emmons, L. K., Lamarque, J.-F., Richter, J. H., Glanville, A. S., Bacmeister, J. T., Phillips, A. S., Neale, R. B., Simpson, I. R., DuVivier, A. K., Hodzic, A., and Randel, W. J.: The Whole Atmosphere Community Climate Model Version 6 (WACCM6), *Journal of Geophysical Research: Atmospheres*, p. 2019JD030943, <https://doi.org/10.1029/2019JD030943>, 2019.

Griffiths, P. T., Murray, L. ~~M. T.~~, Zeng, G. ~~et al.~~, Archibald, A. T., Emmons, L. K., Galbally, I., Hassler, B.,
 835 Horowitz, L. W., Keeble, J., Liu, J., Moeini, O., Naik, V., O'Connor, F. M., Shin, Y. M., Tarasick, D., Tilmes, S., Turnock, S. T., Wild, O., Young, P. J., and Zanis, P.: Tropospheric ozone in CMIP6 *Simulations, Atmos. Chem. Phys. simulations, submitted to Atmospheric Chemistry and Physics-Discuss.*, <https://doi.org/10.5194/acp-2019-1216>, in review, 2020.

~~Holmes, C. D., Prather, M. J., Søvde, O. A., and Myhre, G.: Future methane, hydroxyl, and their uncertainties: key climate and emission parameters for future predictions, *Atmos. Chem. Phys.*, 13, 285–302, <https://doi.org/10.5194/acp-13-285-2013>, 2013~~

~~Gromov, S., Brenninkmeijer, C. A. M., and Jöckel, P.: A very limited role of tropospheric chlorine as a sink of the greenhouse gas methane, *Atmos. Chem. Phys.*, 18, 9831–9843, <https://doi.org/10.5194/acp-18-9831-2018>, 2018.~~

845 ~~He, J., Naik, V., Horowitz, L. W., Dlugokencky, E., and Thoning, K.: Investigation of the global methane budget over 1980–2017 using GFDL-AM4.1, *Atmos. Chem. Phys.*, 20, 805–827, <https://doi.org/10.5194/acp-20-805-2020>, 2020.~~

Hoesly, R. M., S. J. Smith, L. Feng, Z. Klimont, G. Janssens-Maenhout, T. Pitkanen, J. J. Seibert, L. Vu, R. J. Andres, R. M. Bolt, T. C. Bond, L. Dawidowski, N. Kholod, J. Kurokawa, M. Li, L. Liu, Z. Lu, M. C. P. Moura,
 850 P. R. O'Rourke, and Q. Zhang: Historical (1750–2014) anthropogenic emissions of reactive gases and aerosols from the Community Emissions Data System (CEDS), *Geosci. Model Dev.*, 11, 369-408, doi.org/10.5194/gmd-11-369-2018, 2018.

~~Holmes, C. D. (2018). Methane feedback on atmospheric chemistry: Methods, models, and mechanisms. *Journal of Advances in Modeling Earth Systems*, 10, 1087– 1099. <https://doi.org/10.1002/2017MS001196>~~

855 [Holmes, C. D., Prather, M. J., Søvde, O. A., and Myhre, G.: Future methane, hydroxyl, and their uncertainties: key climate and emission parameters for future predictions, *Atmos. Chem. Phys.*, 13, 285–302, <https://doi.org/10.5194/acp-13-285-2013>, 2013](#)

Horowitz, L. W., [Naik, V., Paulot, F., Ginoux, P. A., Dunne, J. P., Mao, J., et al., \(2020\). The GFDL Global Atmospheric Chemistry–Climate Model AM4.1: Model Description and Simulation Characteristics](#), ~~submitted~~,
860 [Journal of Advances in Modeling Earth Systems](#), 12, e2019MS002032. <https://doi.org/10.1029/2019MS002032>

[Hossaini, R., Chipperfield, M. P., Saiz-Lopez, A., Fernandez, R., Monks, S., Feng, W., Brauer, P., and von Glasow, R.: A global model of tropospheric chlorine chemistry: Organic versus inorganic sources and impact on methane oxidation, *J. Geophys. Res.-Atmos.*, 121, 14271–14297, <https://doi.org/10.1002/2016JD025756>, 2016.](#)

865 [IPCC, 2013: Annex II: Climate System Scenario Tables \[Prather, M., G. Flato, P. Friedlingstein, C. Jones, J.-F. Lamarque, H. Liao and P. Rasch \(eds.\)\]. In: Climate Change 2013: The Physical Science Basis. Contribution of Working Group I to JAMES, 2019the Fifth Assessment Report of the Intergovernmental Panel on Climate Change \[Stocker, T.F., D. Qin, G.-K. Plattner, M. Tignor, S.K. Allen, J. Boschung, A. Nauels, Y. Xia, V. Bex and P.M. Midgley \(eds.\)\]. Cambridge University Press, Cambridge, United Kingdom and New York, NY, USA, pp. 1395-1445, 2014.](#)

870 [Isaksen, I.S.A., C. Granier, G. Myhre, T.K. Berntsen, S.B. Dalsøren, M. Gauss, Z. Klimont, R. Benestad, P. Bousquet, W. Collins, T. Cox, V. Eyring, D. Fowler, S. Fuzzi, P. Jöckel, P. Laj, U. Lohmann, M. Maione, P. Monks, A.S.H. Prevot, F. Raes, A. Richter, B. Rognerud, M. Schulz, D. Shindell, D.S. Stevenson, T. Storelvmo, W.-C. Wang, M. van Weele, M. Wild, D. Wuebbles, Atmospheric composition change: Climate–Chemistry interactions, *Atmos. Environ.*, 43\(33\), 5138-5192, <https://doi.org/10.1016/j.atmosenv.2009.08.003>, 2009](#)

875 [Ito, A. & Inatomi, M. Use of a process-based model for assessing the methane budgets of global terrestrial ecosystems and evaluation of uncertainty, *Biogeosciences* 9, 759-773 \(2012\).](#)

[Kirschke, S., Bousquet, P., Ciais, P., Saunois, M., Canadell, J. G., Dlugokencky, E. J., Bergamaschi, P., Bergmann, D., Blake, D. R., Bruhwiler, L., Cameron-Smith, P., Castaldi, S., Chevallier, F., Feng, L., Fraser, A., Heimann, M., Hodson, E. L., Houweling, S., Josse, B., Fraser, P. J., Krummel, P. B., Lamarque, J.-F., Langenfelds, R. L., Le Quere, C., Naik, V., O'Doherty, S., Palmer, P. I., Pison, I., Plummer, D., Poulter, B., Prinn, R. G., Rigby, M., Ringeval, B., Santini, M., Schmidt, M., Shindell, D. T., Simpson, I. J., Spahni, R., Steele, L. P., Strode, S. A., Sudo, K., Szopa, S., van der Werf, G. R., Voulgarakis, A., van Weele, M., Weiss, R. F., Williams, J. E., and Zeng, G.: Three decades of global methane sources and sinks, *Nat. Geosci.*, 6, 813–823, <https://doi.org/10.1038/NGEO1955>, 2013.](#)

880 [Krol, M., and J. Lelieveld \(2003\), Can the variability in tropospheric OH be deduced from measurements of 1,1,1-trichloroethane \(methyl chloroform\)?, *J. Geophys. Res.*, 108\(D3\), 4125, doi:10.1029/2002JD002423.](#)

885 [Krol, M., J. Lelieveld, D. Oram, G. Sturrock, S. Penkett, C. Brenninkmeijer, V. Gros, J. Williams, and H. Scheeren \(2003\), Continuing emissions of methyl chloroform from Europe, *Nature*, 421\(6919\), 131–135, doi:10.1038/nature01311.](#)

~~[Krol, M.C., et al. \(2008\) What can ¹⁴C measurements tell us about OH? *Atmos. Chem. Phys.*, 8, 5033–5044](#)~~

[Lawrence, M. G., Jöckel, P., and von Kuhlmann, R.: What does the global mean OH concentration tell us?, *Atmos. Chem. Phys.*, 1, 37–49, doi:10.5194/acp-1-37-2001, 2001.](#)

- 895 Lelieveld, J., Gromov, S., Pozzer, A., and Taraborrelli, D.: Global tropospheric hydroxyl distribution, budget and reactivity, *Atmos. Chem. Phys.*, 16, 12477–12493, <https://doi.org/10.5194/acp-16-12477-2016>, 2016.
- Lovelock, J. E. (1977), Methyl chloroform in the troposphere as an indicator of OH radical abundance, *Nature*, 267(5606), 32 pp.
- 900 [McNorton, J., Chipperfield, M. P., Gloor, M., Wilson, C., Feng, W., Hayman, G. D., Rigby, M., Krummel, P. B., O'Doherty, S., Prinn, R. G., Weiss, R. F., Young, D., Dlugokencky, E., and Montzka, S. A.: Role of OH variability in the stalling of the global atmospheric CH₄ growth rate from 1999 to 2006, *Atmos. Chem. Phys.*, 16, 7943–7956, <https://doi.org/10.5194/acp-16-7943-2016>, 2016.](#)
- 905 [McNorton, J., Wilson, C., Gloor, M., Parker, R. J., Boesch, H., Feng, W., Hossaini, R., and Chipperfield, M. P.: Attribution of recent increases in atmospheric methane through 3-D inverse modelling, *Atmos. Chem. Phys.*, 18, 18149–18168, <https://doi.org/10.5194/acp-18-18149-2018>, 2018.](#)
- Meinshausen, M., E. Vogel, A. Nauels, K. Lorbacher, N. Meinshausen, D. M. Etheridge, P. J. Fraser, S. A. Montzka, P. J. Rayner, C. M. Trudinger, P. B. Krummel, U. Beyerle, J. G. Canadell, J. S. Daniel, I. G. Enting, R. M. Law, C. R. Lunder, S. O'Doherty, R. G. Prinn, S. Reimann, M. Rubino, G. J. M. Velders, M. K. Vollmer, R. H. J. Wang, and R. Weiss: Historical greenhouse gas concentrations for climate modelling (CMIP6), *Geosci. Model Dev.*, 10, 2057–2116, doi.org/10.5194/gmd-10-2057-2017, 2017
- 910 [Miyazaki, K., Eskes, H. J., and Sudo, K.: A tropospheric chemistry reanalysis for the years 2005–2012 based on an assimilation of OMI, MLS, TES, and MOPITT satellite data, *Atmos. Chem. Phys.*, 15, 8315–8348, <https://doi.org/10.5194/acp-15-8315-2015>, 2015](#)
- 915 [Miyazaki, K., Eskes, H., Sudo, K., Boersma, K. F., Bowman, K., and Kanaya, Y.: Decadal changes in global surface NO_x emissions from multi-constituent satellite data assimilation, *Atmos. Chem. Phys.*, 17, 807–837, <https://doi.org/10.5194/acp-17-807-2017>, 2017](#)
- [Miyazaki, K. and Bowman, K.: Evaluation of ACCMIP ozone simulations and ozonesonde sampling biases using a satellite-based multi-constituent chemical reanalysis, *Atmos. Chem. Phys.*, 17, 8285–8312, <https://doi.org/10.5194/acp-17-8285-2017>, 2017](#)
- 920 Montzka, S., C. Spivakovsky, J. Butler, J. Elkins, L. Lock, and D. Mondeel (2000), New observational constraints for atmospheric hydroxyl on global and hemispheric scales, *Science*, 288(5465), 500–503.
- Montzka, S. A., M. Krol, E. Dlugokencky, B. Hall, P. Joeckel, and J. Lelieveld (2011), Small interannual variability of global atmospheric hydroxyl, *Science*, 331(6013), 67–69, [doi:10.1126/science.1197640](https://doi.org/10.1126/science.1197640).
- 925 Mulcahy, J. P., Johnson C., Jones C., Povey A., Sellar A., Scott C. E., Turnock S. T., Woodhouse M. T., Abraham L. N., Andrews M., Bellouin N., Browse J., Carslaw K. S., Dalvi M., Folberth G., Grosvenor D., Hardacre C., Johnson B., Jones A., Kipling Z., Mann G., Mollard J., Schutgens N., O'Connor F., Palmieri J., Reddington C., Richardson M., Stier P., Woodward S., and Yool A.: Description and evaluation of aerosol in UKESM1 and HadGEM3-GC3.1 CMIP6 historical simulations, *Geosci. Model. Dev.*, In preparation, 2019.
- 930 Murray, L. T., Mickley, L. J., Kaplan, J. O., Sofen, E. D., Pfeiffer, M., and Alexander, B.: Factors controlling variability in the oxidative capacity of the troposphere since the Last Glacial Maximum, *Atmos. Chem. Phys.*, 14, 3589–3622, <https://doi.org/10.5194/acp-14-3589-2014>, 2014.
- Naik, V., Voulgarakis, A., Fiore, A. M., Horowitz, L. W., Lamarque, J.-F., Lin, M., Prather, M. J., Young, P. J., Bergmann, D., Cameron-Smith, P. J., Cionni, I., Collins, W. J., Dalsøren, S. B., Doherty, R., Eyring, V., Faluvegi, G., Folberth, G. A., Josse, B., Lee, Y. H., MacKenzie, I. A., Nagashima, T., van Noije, T. P. C., Plummer, D. A.,

- 935 Righi, M., Rumbold, S. T., Skeie, R., Shindell, D. T., Stevenson, D. S., Strode, S., Sudo, K., Szopa, S., and Zeng, G.: Preindustrial to present-day changes in tropospheric hydroxyl radical and methane lifetime from the Atmospheric Chemistry and Climate Model Intercomparison Project (ACCMIP), *Atmos. Chem. Phys.*, 13, 5277–5298, doi:10.5194/acp-13-5277-2013, 2013.
- 940 [Nguyen, N. H., Turner, A. J., Yin, Y., Prather, M. J., & Frankenberg, C. \(2020\). Effects of chemical feedbacks on decadal methane emissions estimates. *Geophysical Research Letters*, 47, e2019GL085706. <https://doi.org/10.1029/2019GL085706>](#)
- Nicely, J. M., Canty, T. P., Manyin, M., Oman, L. D., Salawitch, R. J., Steenrod, S. D., et al.: Changes in global tropospheric OH expected as a result of climate change over the last several decades. *Journal of Geophysical Research: Atmospheres*, 123, 10,774– 10,795. <https://doi.org/10.1029/2018JD028388>, 2018.
- 945 Nicely, J. M., Duncan, B. N., Hanisco, T. F., Wolfe, G. M., Salawitch, R. J., Deushi, M., Haslerud, A. S., Jöckel, P., Josse, B., Kinnison, D. E., Klekociuk, A., Manyin, M. E., Marécal, V., Morgenstern, O., Murray, L. T., Myhre, G., Oman, L. D., Pitari, G., Pozzer, A., Quaglia, I., Revell, L. E., Rozanov, E., Stenke, A., Stone, K., Strahan, S., Tilmes, S., Tost, H., Westervelt, D. M., and Zeng, G.: A Machine Learning Examination of Hydroxyl Radical Differences Among Model Simulations for CCM1-1, *Atmos. Chem. Phys. Discuss.*, <https://doi.org/10.5194/acp-2019-772>, in review, 2019.
- 950 Naus, S., Montzka, S. A., Pandey, S., Basu, S., Dlugokencky, E. J., and Krol, M.: Constraints and biases in a tropospheric two-box model of OH, *Atmos. Chem. Phys.*, 19, 407–424, <https://doi.org/10.5194/acp-19-407-2019>, 2019
- Patra, P., Krol, M., Montzka, S. et al.: Observational evidence for interhemispheric hydroxyl-radical parity. *Nature* 955 513, 219–223, doi:10.1038/nature13721, 2014.
- Prather, M.J.: Natural modes and time scales in atmospheric chemistry: theory, GWPs for CH₄ and CO, and runaway growth, *Geophys.Res.Lett.*, 23, 2597-2600, 1996.
- Prather, M., D. Ehhalt, F. Dentener, R. G. Derwent, E. Dlugokencky, E. Holland, I. S. A. Isaksen, J. Katima, V. Kirchhoff, P. Matson, P. M. Midgley, and M. Wang: Chapter 4. Atmospheric Chemistry and Greenhouse Gases, 960 in *Climate Change 2001: The Scientific Basis*, J.T. Houghton et al., eds., Cambridge U. Press, pp. 239-287, 2001.
- Prather, M. J., Holmes, C. D., and Hsu, J.: Reactive greenhouse gas scenarios: Systematic exploration of uncertainties and the role of atmospheric chemistry, *Geophys. Res. Lett.*, 39, L09803, doi:10.1029/2012GL051440, 2012.
- Prinn, R., et al.: Evidence for substantial variations of atmospheric hydroxyl radicals in the past two decades, 965 *Science*, 292(5523), 1882–1888, 2001.
- Prinn, R. G., et al.: Evidence for variability of atmospheric hydroxyl radicals over the past quarter century, *Geophys. Res. Lett.*, 32, L07809, doi:10.1029/2004GL022228, 2005.
- Rigby M, et al.: Role of atmospheric oxidation in recent methane growth. *Proc Natl Acad Sci USA* 114:5373–5377, 2017.
- 970 Sellar, A. A., C. G. Jones,, J. Mulcahy, Y. Tang, A. Yool, A. Wiltshire, F. M. O’Connor, M. Stringer, R. Hill, J. Palmieri, S. Woodward, L. de Mora, T. Kuhlbrodt, S. Rumbold, D. I. Kelley, R. Ellis, C. E. Johnson, J. Walton, N. L. Abraham, M. B. Andrews, T. Andrews, A. T. Archibald, S. Berthou, E. Burke, E. Blockley, K. Carslaw, M. Dalvi, J. Edwards, G. A. Folberth, N. Gedney, P. T. Griffiths, A. B. Harper, M. A. Hendry, A. J. Hewitt, B. Johnson, A. Jones, C. D. Jones, J. Keeble, S. Liddicoat, O. Morgenstern, R. J. Parker, V. Predoi, E. Robertson, A.

975 Siahayan, R. S. Smith, R. Swaminathan, M. Woodhouse, G. Zeng, and M. Zerroukat (2019): UKESM1: Description and evaluation of the UK Earth System Model, *J. Adv. Modeling Earth Sys.*, doi.org/10.1029/2019MS001739.

[Sherwen, T., Schmidt, J. A., Evans, M. J., Carpenter, L. J., Großmann, K., Eastham, S. D., Jacob, D. J., Dix, B., Koenig, T. K., Sinreich, R., Ortega, I., Volkamer, R., Saiz-Lopez, A., PradosRoman, C., Mahajan, A. S., and Ordóñez, C.: Global impacts of tropospheric halogens \(Cl, Br, I\) on oxidants and composition in GEOS-Chem, *Atmos. Chem. Phys.*, 16, 12239–12271, <https://doi.org/10.5194/acp-16-12239-2016>, 2016.](#)

980 Singh, H.: Preliminary estimation of average tropospheric HO concentrations in the northern and southern hemispheres, *Geophys. Res. Lett.*, 4(10), 453–456, 1977.

[Spahni, R., Wania, R., Neef, L., van Weele, M., Pison, I., Bousquet, P., Frankenberg, C., Foster, P. N., Joos, F., Prentice, I. C., and van Velthoven, P.: Constraining global methane emissions and uptake by ecosystems, *Biogeosciences*, 8, 1643–1665, <https://doi.org/10.5194/bg-8-1643-2011>, 2011.](#)

985 Spivakovsky, C. M., R. Yevich, J. A. Logan, S. C. Wofsy, M. B. McElroy, and M. J. Prather, Tropospheric OH in a three-dimensional chemical tracer model: An assessment based on observations of CH₃ CCl₃, *J. Geophys. Res.*, 95, 18,441–18,471, 1990.

Spivakovsky, C., et al.: Three-dimensional climatological distribution of tropospheric OH: Update and evaluation, *J. Geophys. Res.*, 105, 8931–8980, 2000.

990 Stevenson, D. S., Young, P. J., Naik, V., Lamarque, J.-F., Shindell, D. T., Voulgarakis, A., Skeie, R. B., Dalsoren, S. B., Myhre, G., Bernsten, T. K., Folberth, G. A., Rumbold, S. T., Collins, W. J., MacKenzie, I. A., Doherty, R. M., Zeng, G., van Noije, T. P. C., Strunk, A., Bergmann, D., Cameron-Smith, P., Plummer, D. A., Strode, S. A., Horowitz, L., Lee, Y. H., Szopa, S., Sudo, K., Nagashima, T., Josse, B., Cionni, I., Righi, M., Eyring, V., Conley, A., Bowman, K. W., Wild, O., and Archibald, A.: Tropospheric ozone changes, radiative forcing and attribution to emissions in the Atmospheric Chemistry and Climate Model Intercomparison Project (ACCMIP), *Atmos. Chem. Phys.*, 13, 3063–3085, <https://doi.org/10.5194/acp-13-3063-2013>, 2013.

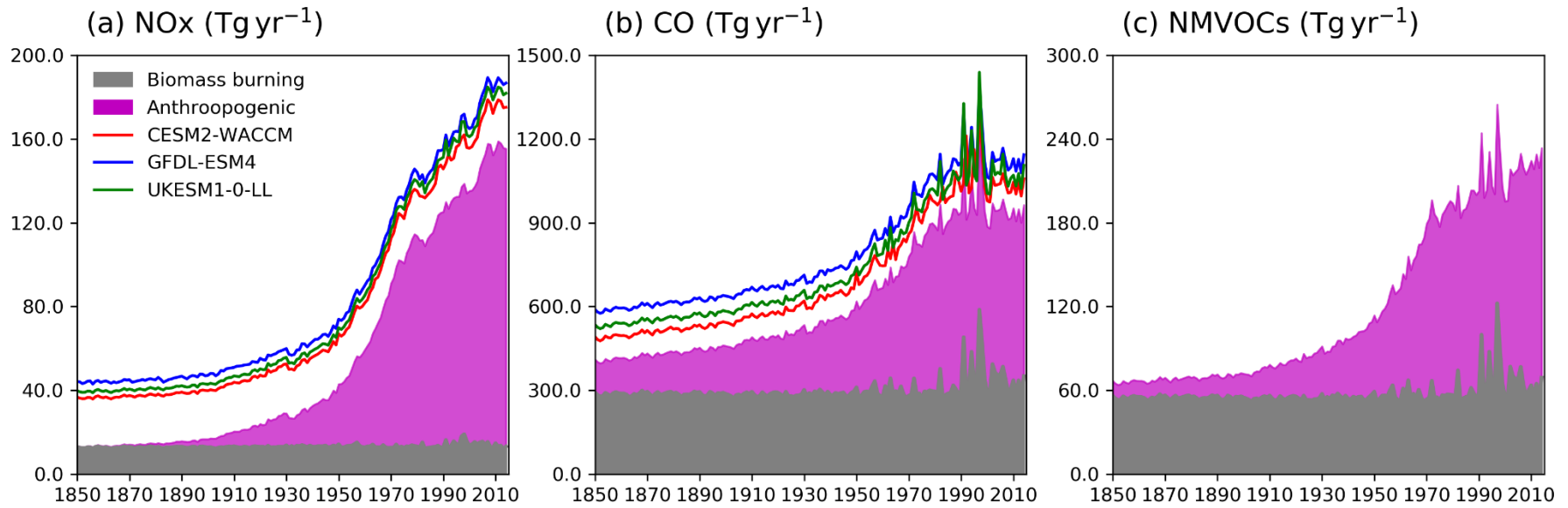
Stone, D., Whalley, L.K., and Heard, D.E.: Tropospheric OH and HO₂ radicals: field measurements and model comparisons, *Chemical Society Reviews* 41 (19), 6348-6404, 2012.

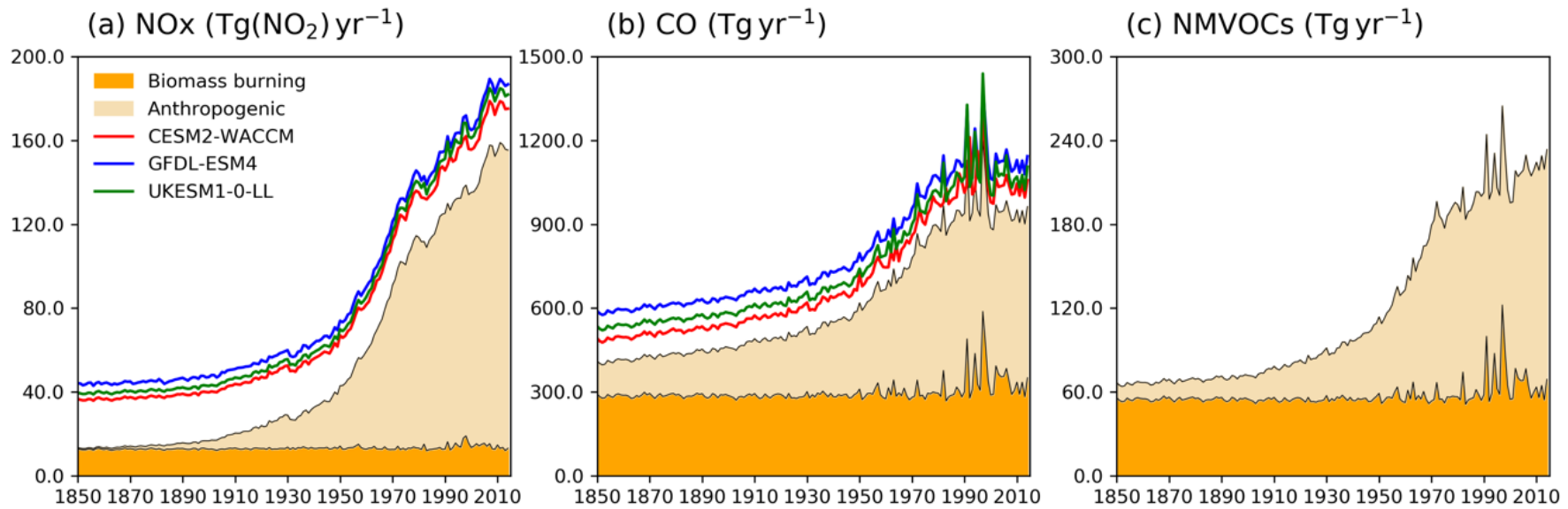
1000 [Strode, S. A., Wang, J. S., Manyin, M., Duncan, B., Hossaini, R., Keller, C. A., Michel, S. E., and White, J. W. C.: Strong sensitivity of the isotopic composition of methane to the plausible range of tropospheric chlorine, *Atmos. Chem. Phys.*, 20, 8405–8419, <https://doi.org/10.5194/acp-20-8405-2020>, 2020.](#)

Thornhill, G. D., Collins, W. J., Kramer, R. J., Olivíe, D., ~~O'Connor~~ O'Connor, F., Abraham, N. L., Bauer, S. E., Deushi, M., Emmons, L., Forster, P., Horowitz, L., Johnson, B., Keeble, J., Lamarque, J.-F., Michou, M., Mills, M., Mulcahy, J., Myhre, G., Nabat, P., Naik, V., Oshima, N., Schulz, M., Smith, C., Takemura, T., Tilmes, S., Wu, T., Zeng, G., and Zhang, J.: Effective Radiative forcing from emissions of reactive gases and aerosols – a ~~multi model~~ multimodel comparison, *Submitted to Atmos. Chem. Phys. Discuss.*, <https://doi.org/10.5194/acp-2019-1205>, in review, 2020a.

1005 [Thornhill, G., Collins, W., Olivíe, D., Archibald, A., Bauer, S., Checa-Garcia, R., Fiedler, S., Folberth, G., Gjermundsen, A., Horowitz, L., Lamarque, J.-F., Michou, M., Mulcahy, J., Nabat, P., Naik, V., O'Connor, F. M., Paulot, F., Schulz, M., Scott, C. E., Seferian, R., Smith, C., Takemura, T., Tilmes, S., and Weber, J.: Climate-driven chemistry and aerosol feedbacks in CMIP6 Earth system models, *Atmos. Chem. Phys. Discuss.*, <https://doi.org/10.5194/acp-2019-1207>, in review, 2020b.](#)

- 1015 [Tian, H. et al. Global methane and nitrous oxide emissions from terrestrial ecosystems due to multiple environmental changes. *Ecosystem Health and Sustainability* 1, art4, doi:10.1890/EHS14-0015.1 \(2015\).](#)
- [Tian, H., Lu, C., Ciais, P. et al. The terrestrial biosphere as a net source of greenhouse gases to the atmosphere. *Nature* 531, 225–228 \(2016\). <https://doi.org/10.1038/nature16946>](#)
- Turner, A.J., C. Frankenberg, P.O. Wennberg, and D.J. Jacob: Ambiguity in the causes for decadal trends in atmospheric methane and hydroxyl, *Proc. Natl. Acad. Sci.*, 114, 5367-5372, doi:10.1073/pnas.1616020114, 2017.
- 1020 Turner, A.J., I. Fung, V. Naik, L.W. Horowitz, and R.C. Cohen: Modulation of hydroxyl variability by ENSO in the absence of external forcing, *Proc. Natl. Acad. Sci.*, 115, 8931-8936, doi:10.1073/pnas.1807532115, 2018.
- Turner, A.J., C. Frankenberg, and E.A. Kort: Interpreting contemporary trends in atmospheric methane, *Proc. Natl. Acad. Sci.*, 116, 2805-2813, doi:10.1073/pnas.1814297116, 2019.
- 1025 [Turnock, S. T., Allen, R. J., Andrews, M., Bauer, S. E., Emmons, L., Good, P., Horowitz, L., Michou, M., Nabat, P., Naik, V., Neubauer, D., O'Connor, F. M., Olivić, D., Schulz, M., Sellar, A., Takemura, T., Tilmes, S., Tsigaridis, K., Wu, T., and Zhang, J.: Historical and future changes in air pollutants from CMIP6 models, *Atmos. Chem. Phys. Discuss.*, <https://doi.org/10.5194/acp-2019-1211>, in review, 2020.](#)
- van Marle, M. J. E., S. Kloster, B. I. Magi, J. R. Marlon, A.-L. Daniau, R. D. Field, A. Arneth, M. Forrest, S. Hantson, N. M. Kehrwald, W. Knorr, G. Lasslop, F. Li, S. Mangeon, C. Yue, J. W. Kaiser, and G. R. van der Werf: Historic global biomass burning emissions for CMIP6 (BB4CMIP) based on merging satellite observations with proxies and fire models (1750–2015), *Geosci. Model Dev.*, 10, 3329-3357, doi.org/10.5194/gmd-10-3329-2017, 2017.
- 1030 Voulgarakis, A., Naik, V., Lamarque, J.-F., Shindell, D. T., Young, P. J., Prather, M. J., Wild, O., Field, R. D., Bergmann, D., Cameron-Smith, P., Cionni, I., Collins, W. J., Dalsøren, S. B., Doherty, R. M., Eyring, V., Faluvegi, G., Folberth, G. A., Horowitz, L. W., Josse, B., McKenzie, I. A., Nagashima, T., Plummer, D. A., Righi, M., Rumbold, S. T., Stevenson, D. S., Strode, S. A., Sudo, K., Szopa, S., and Zeng, G.: Analysis of present day and future OH and methane lifetime in the ACCMIP simulations, *Atmos. Chem. Phys.*, 13, 2563-2587, doi:10.5194/acp-13-2563-2013, 2013.
- 1035 [Wang, X., Jacob, D. J., Eastham, S. D., Sulprizio, M. P., Zhu, L., Chen, Q., Alexander, B., Sherwen, T., Evans, M. J., Lee, B. H., Haskins, J. D., Lopez-Hilfiker, F. D., Thornton, J. A., Huey, G. L., and Liao, H.: The role of chlorine in global tropospheric chemistry, *Atmos. Chem. Phys.*, 19, 3981–4003, <https://doi.org/10.5194/acp-19-3981-2019>, 2019.](#)
- Wild, O., Voulgarakis, A., O'Connor, F., Lamarque, J.-F., Ryan, E. M., and Lee, L.: Global sensitivity analysis of chemistry-climate model budgets of tropospheric ozone and OH: Exploring model diversity, *Atmos. Chem. Phys. Discuss.*, <https://doi.org/10.5194/acp-2019-774>, in review, 2019.
- 1045

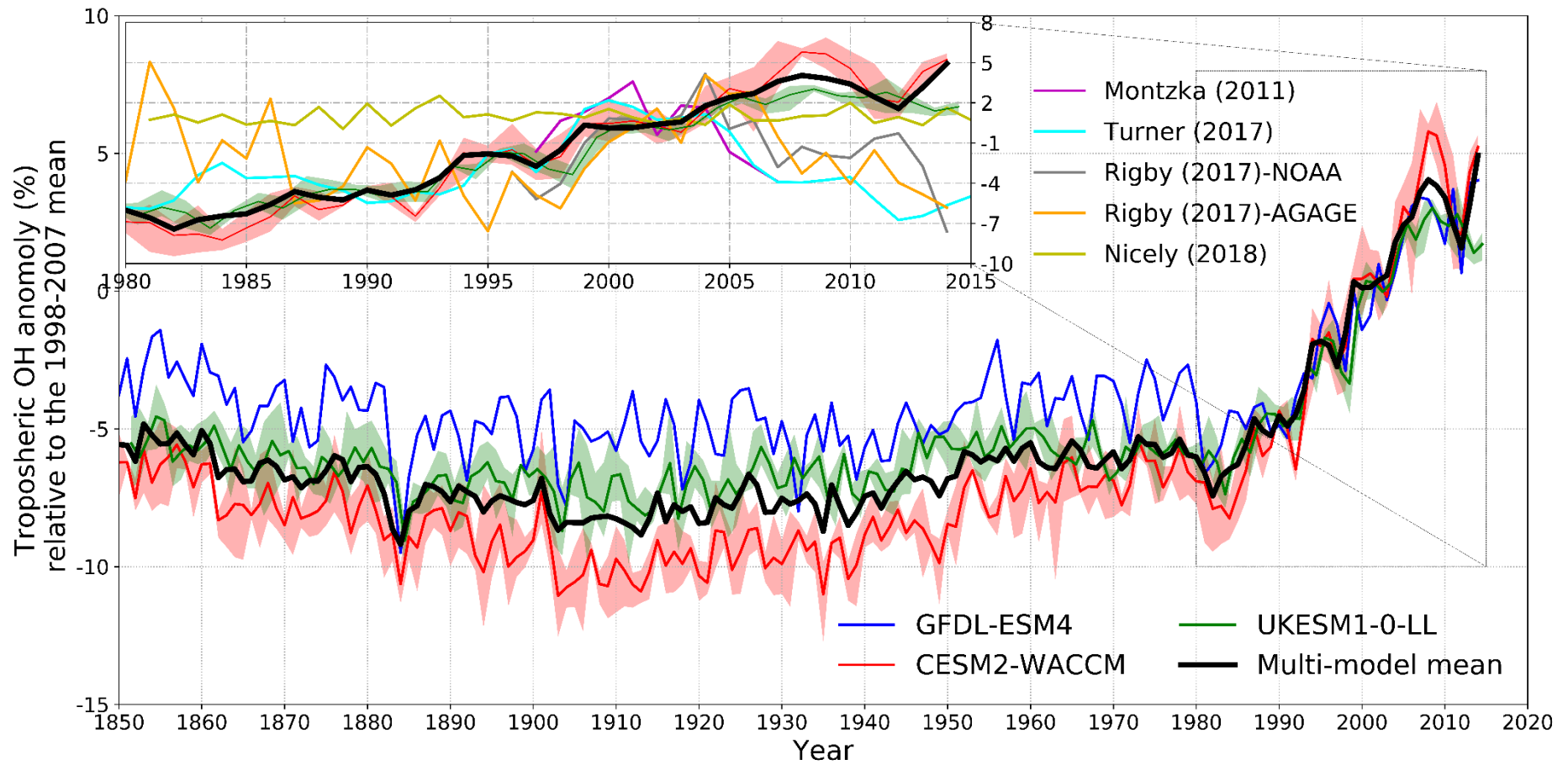




049

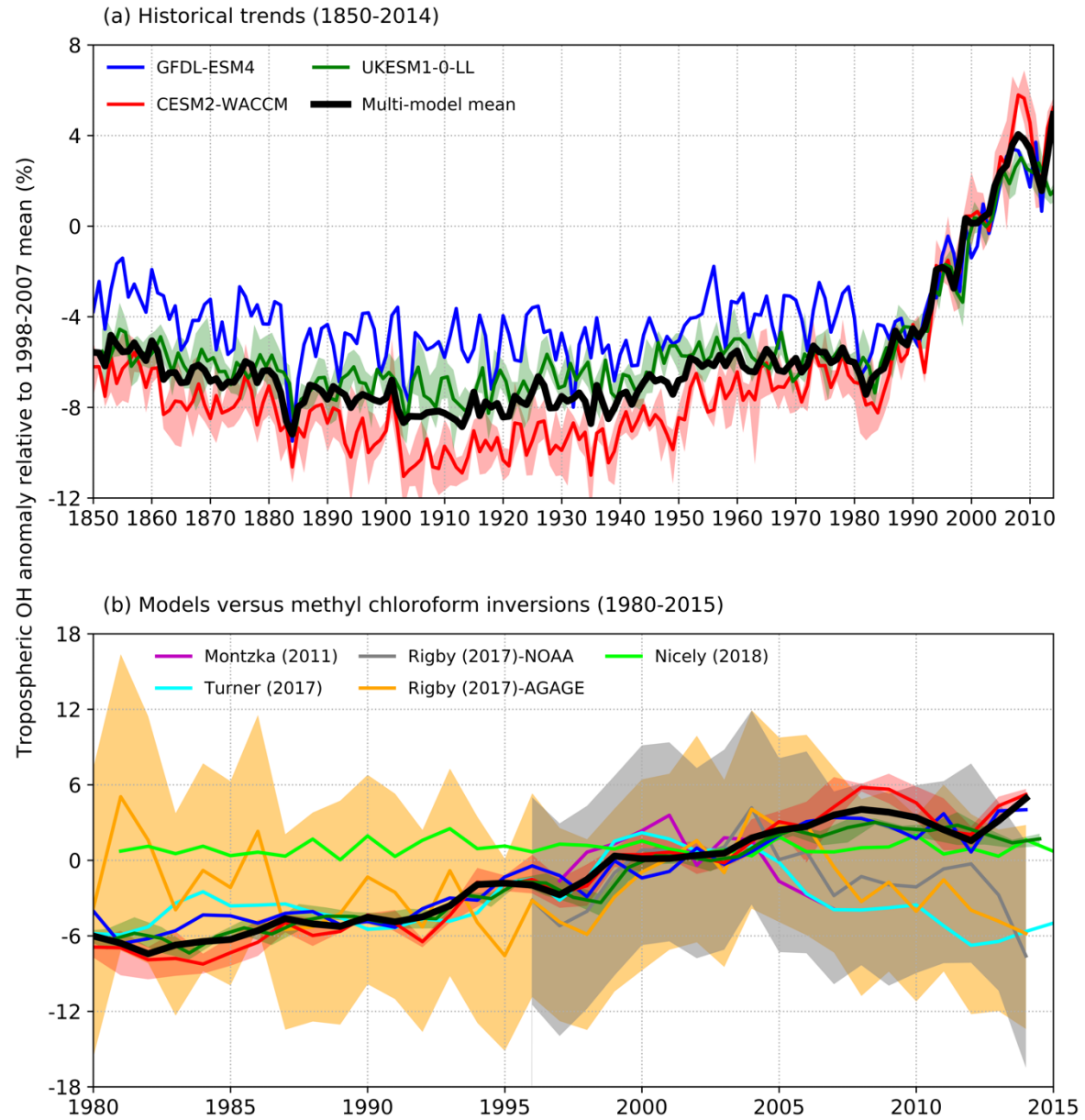
050 Figure 1. Time evolution (1850-2014) of global total ~~emission~~emissions for: (a) NOx (Tg(NO₂) yr⁻¹); (b) CO (Tg(CO) yr⁻¹); and (c) NMVOC (Tg(VOC) yr⁻¹). ~~Grey~~Orange for biomass
 051 burning, ~~purple~~grey for anthropogenic emissions. (Hoesly et al., 2018). The coloured lines in the NOx and CO panels (red for CESM2-WACCM, blue for GFDL-ESM4, and green for
 052 UKESM1-0-LL) are the total ~~emission-used in~~emissions for each model ~~with, including~~ natural ~~emissions-included-sources~~ sources. For historical biogenic VOC emissions, see Griffiths et al.
 053 (2020, Figure 1).

054



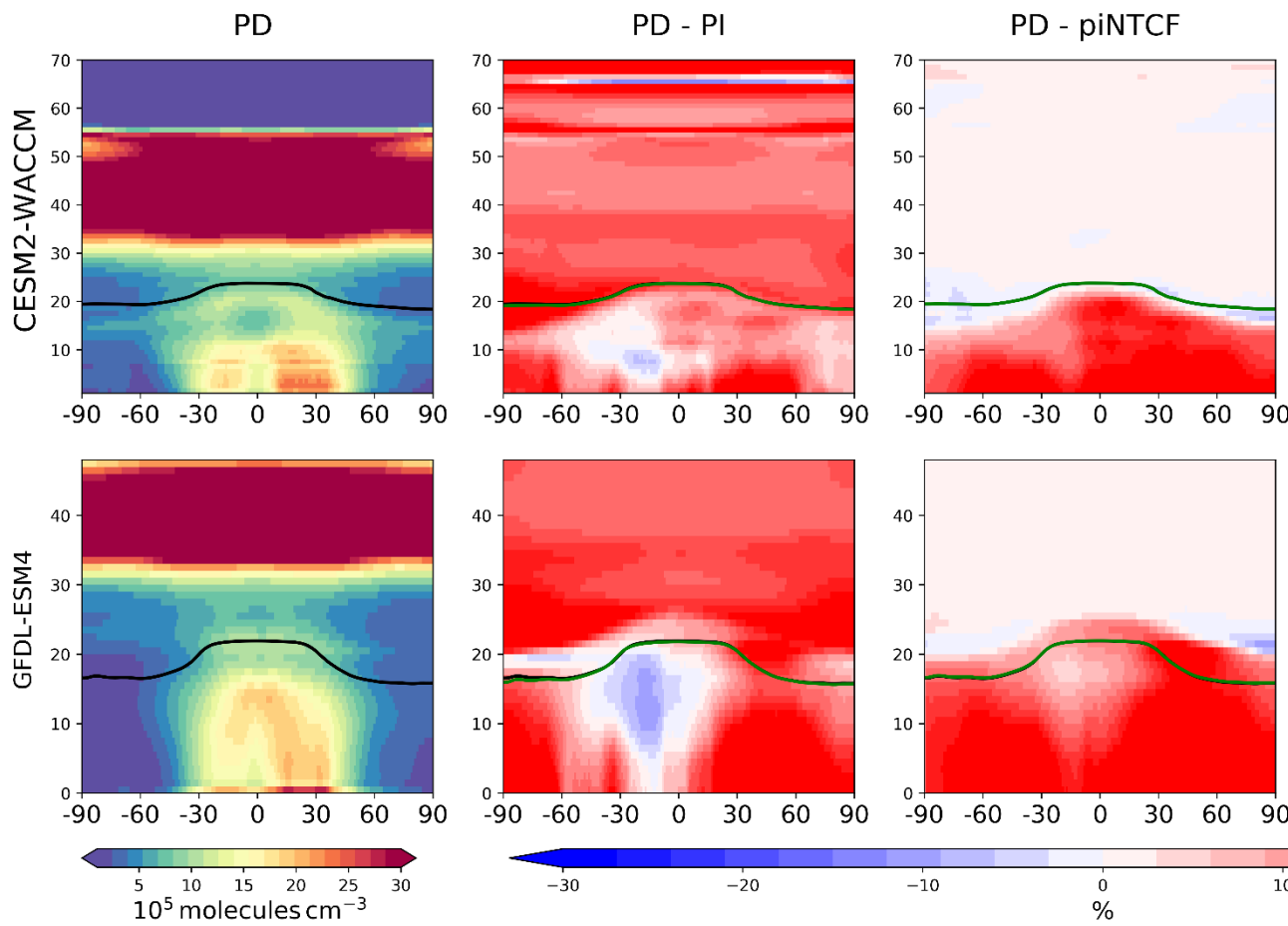
1055
1056

|057

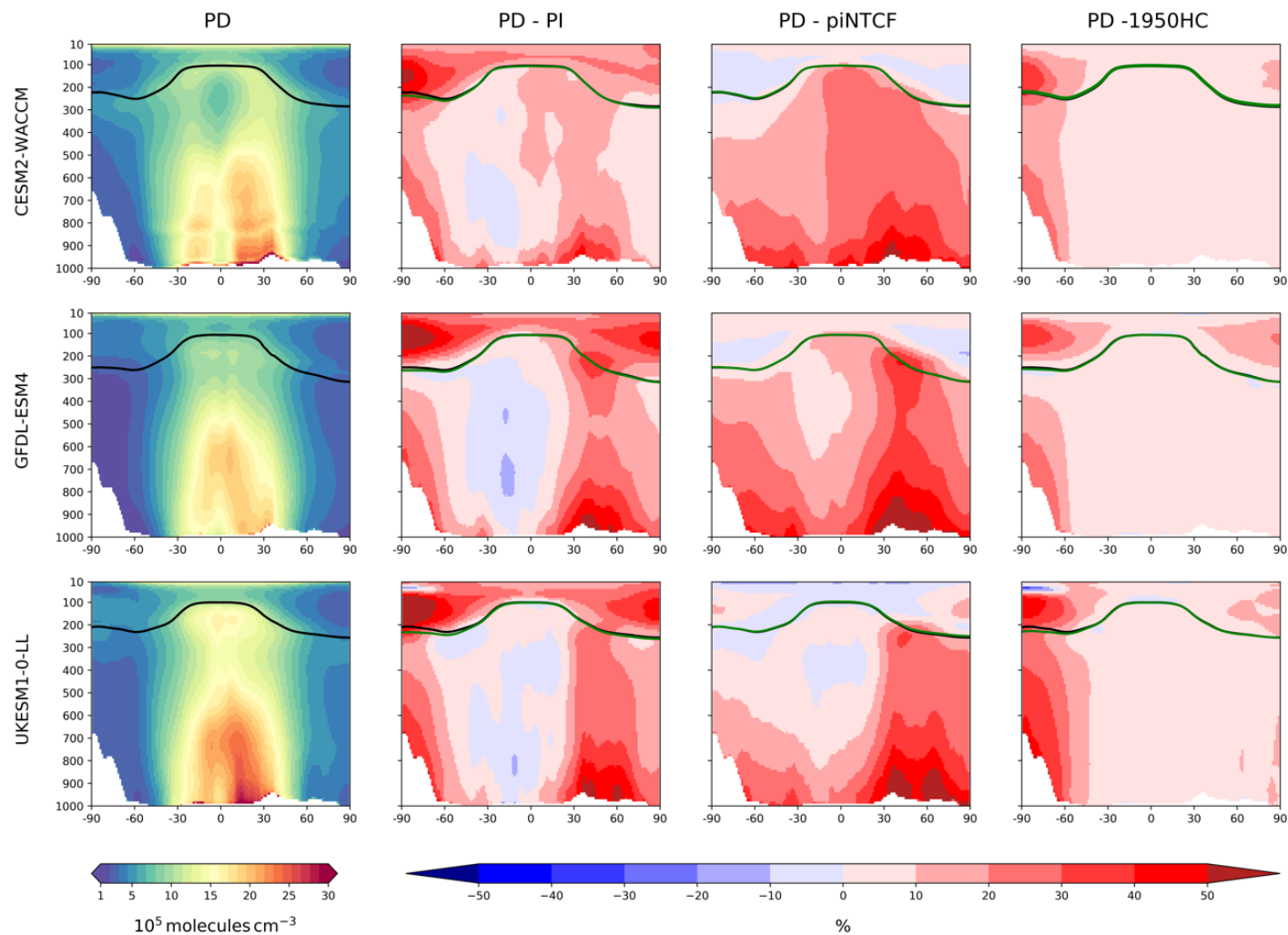


059 **Figure 2. (a) Time evolution (~~1850-2014~~) of global annual mean tropospheric OH₇ (~~1850-2014~~), expressed as a percentage anomaly relative to the 1998-2007 mean ~~value~~ (and ensemble**
060 **spreads, where available for UKESM1-0-LL (green), GFDL-ESM4 (blue), UKESM1-0-LL (green), and CESM2-WACCM (red). ~~Other data in~~, and the zoomed box (1980-2015) are**
061 **observation multi-model mean (black). (b) Observation-based inversions: of global annual mean tropospheric OH for 1980-2015 from Montzka et al. (2011), Rigby et al., 2017, Turner**
062 **et al., 2017, and Nicely et al. (2018), including ±1 standard deviation uncertainties for the results from Rigby et al. (2017), with model results from panel (a) overlain.**

|063



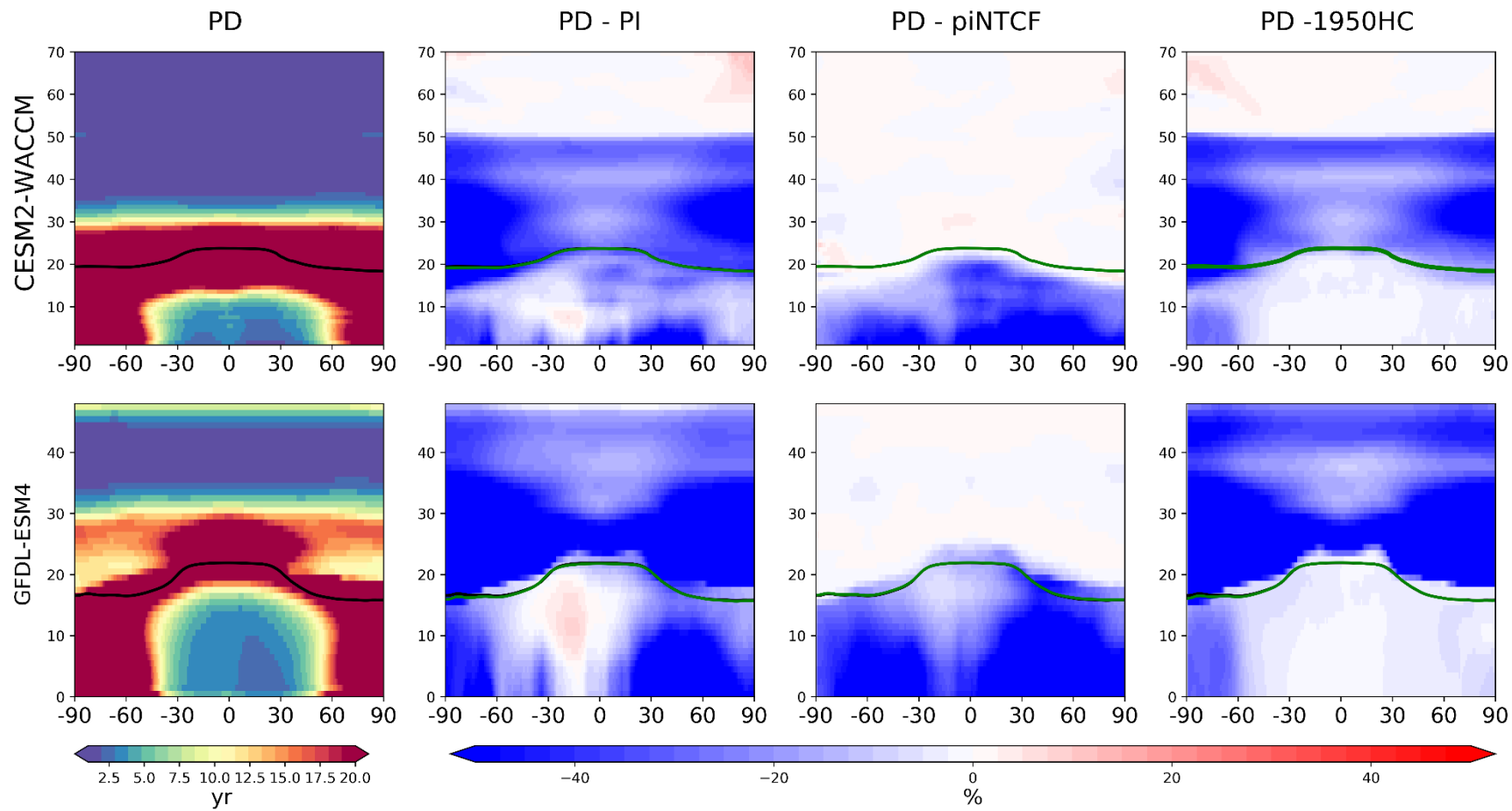
1064



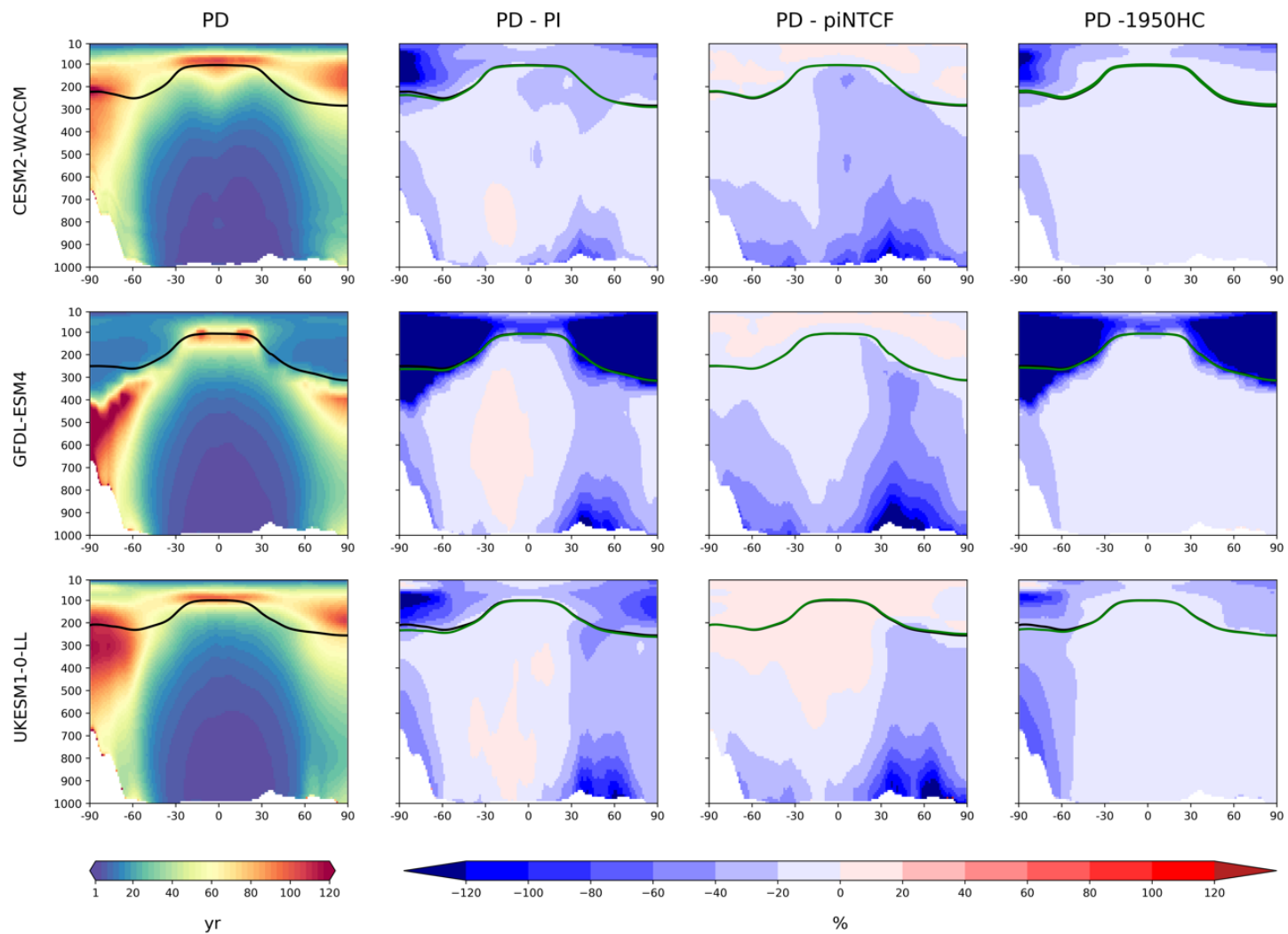
065

066 **Figure 3-Zonal. First column: zonal mean (latitude/model vertical level)-pressure (hPa) cross sections for (first column)-OH concentration (10^5 molecules cm^{-3}) averaged over the**
 067 **period 2005-2014 (PD), and, in the for the histSST simulations. Rows show results for CESM2-WACCM, GFDL-ESM4 and UKESM1-0-LL. Solid lines indicate the tropopause (PD**
 068 **in black; other in green). Other panels, show differences (%) between experiments-expressed as percentage changes. They are, (second, Second column): histSST PD (2005-2014 mean)**

069 minus PI (1850-1859 mean); ~~(third. Third column) PD (2005-2014 mean); histSST minus histSST-piNTCF (2005-2014 mean); and (fourthfor PD. Fourth column) PD (2005-2014~~
070 ~~mean); histSST minus histSST-1950HC (2005-2014 mean). Top for CESM2-WACCM and bottom for GFDL-ESM4. See Figure S6 for changes in absolute valuesfor PD.~~



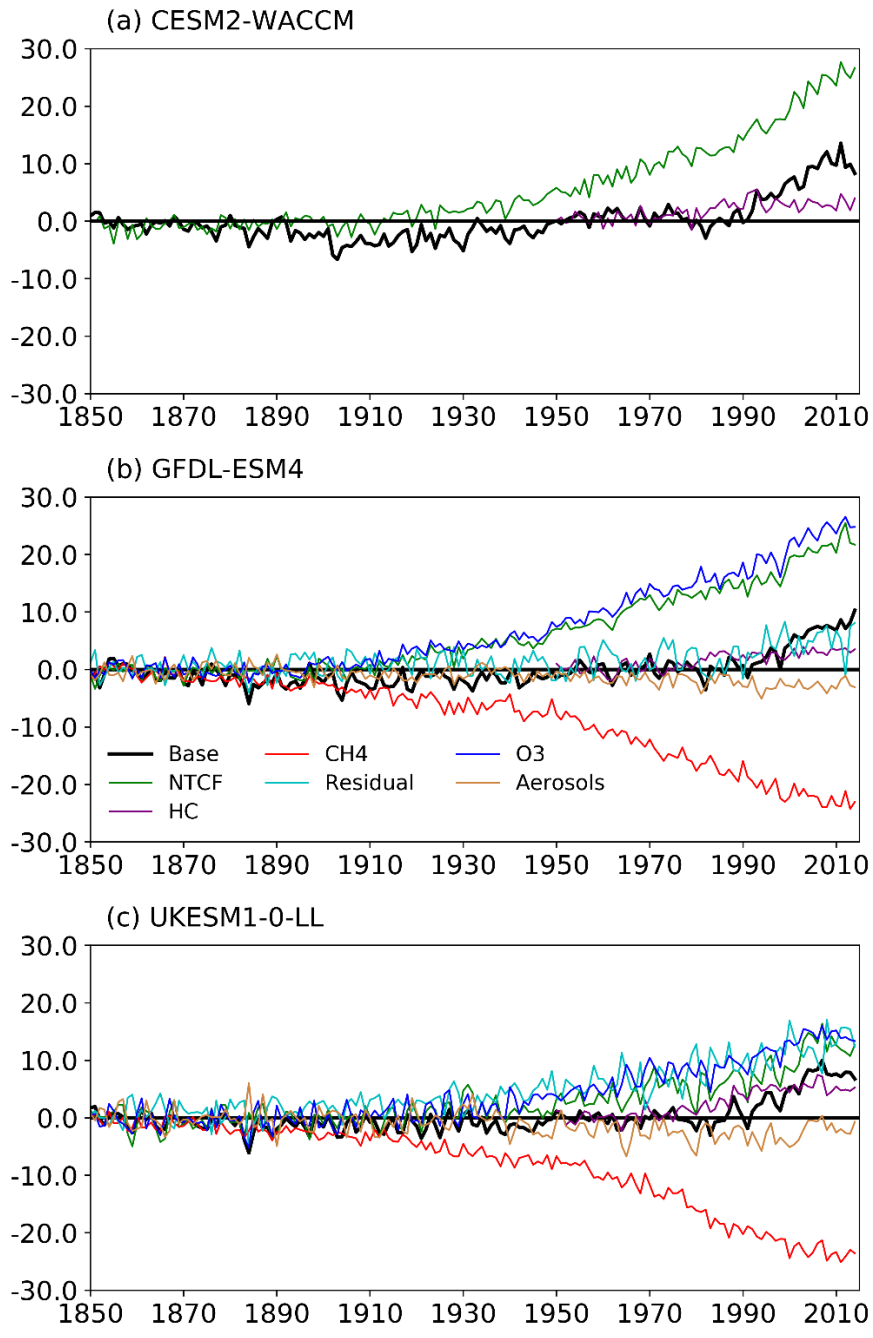
071



072

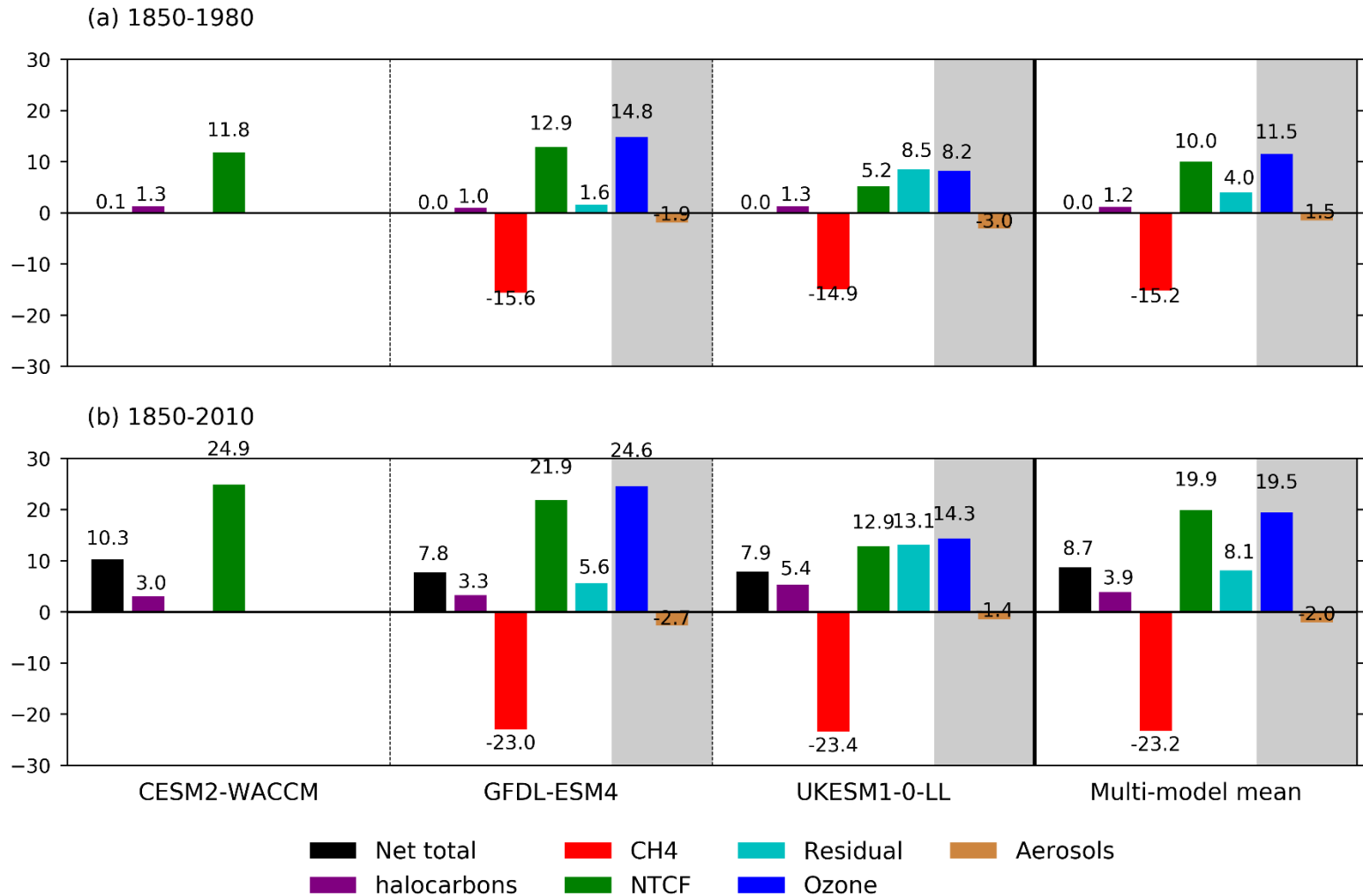
073

Figure 4 The same layout as Figure 3, but for CH₄ lifetime (yr) and the relative.



074
075
076
077
078
079
080

Figure 5. The histSST (Base, in black) tropospheric OH anomaly (% change relative to PI) for each year (see Equation 3), for the three models (a) CESM2-WACCM; (b) GFDL-ESM4; and (c) UKESM1-0-LL. The coloured lines represent the contributions to this OH anomaly due to changes since 1850 in CH₄ mole fraction, NTCF emissions, halocarbon mole fraction, O₃ precursor emissions, and aerosols (see Equations 4-8; NB only NTCF and HC experiments from CESM2-WACCM). The residual curve (see Equation 9) is the extra contribution required after linearly adding the curves for CH₄, NTCF and HC that is needed to reproduce the Base anomaly.



081

082

083

084

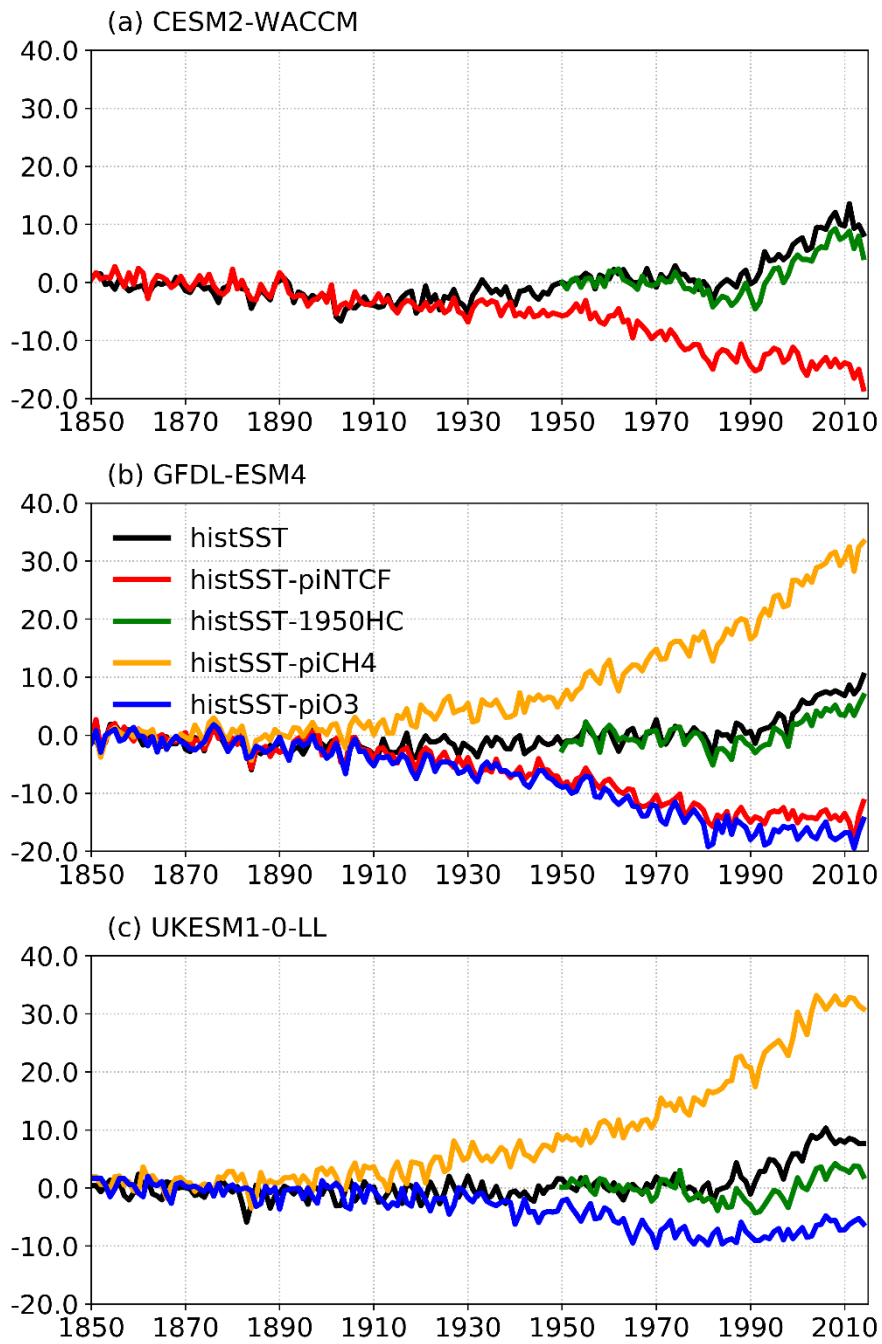
085

086

Figure 6. Summary of drivers of OH changes (%), relative to 1850, for the three models and their multi-model mean over: (a) 1850-1980; and (b) 1850-2010. (NB we have used decadal means: 1850 refers to (1850-1859); 1980 is (1975-1984); and 2010 is (2005-2014). The shaded areas show the split of the NTCF signal (green) into ozone precursors (blue) and aerosols (brown), where models have performed both the histSST-piNTCF and histSST-piO3 experiments. The residual values (pale blue) are the differences between the total change (black, from the histSST simulations) and the sum of the changes. See Figure S8 for changes in absolute values from CH4 (red), NTCF, and halocarbons (purple). We interpret the residual terms as being due to climate change, in addition to any non-linear interactions between forcings.

|087

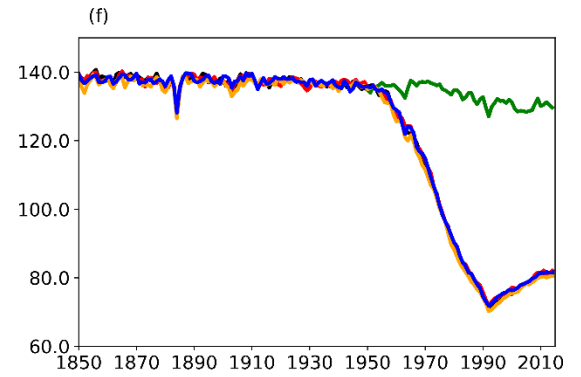
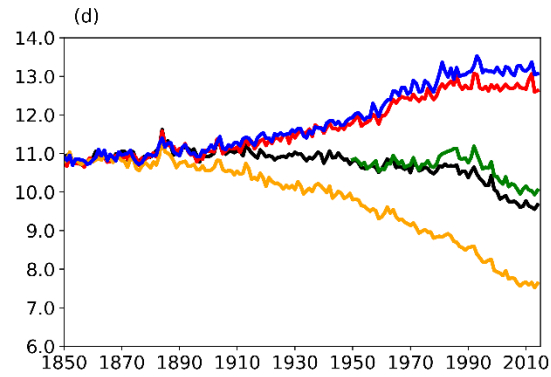
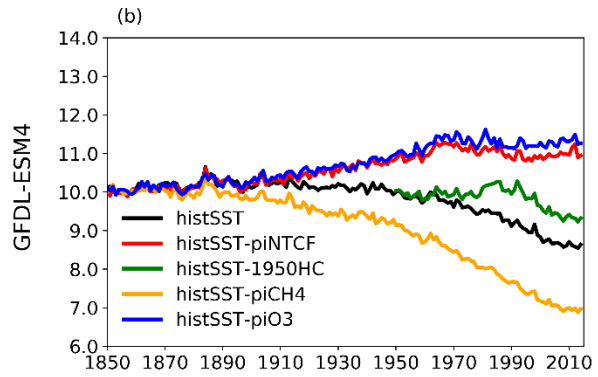
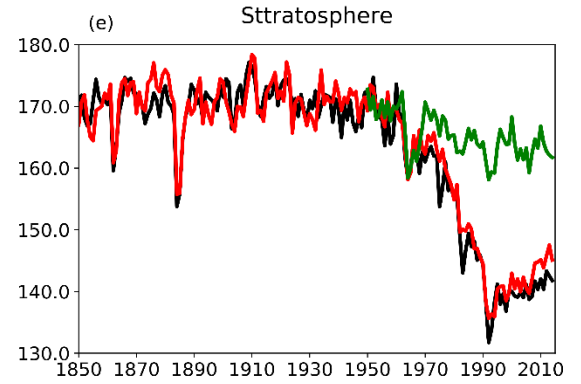
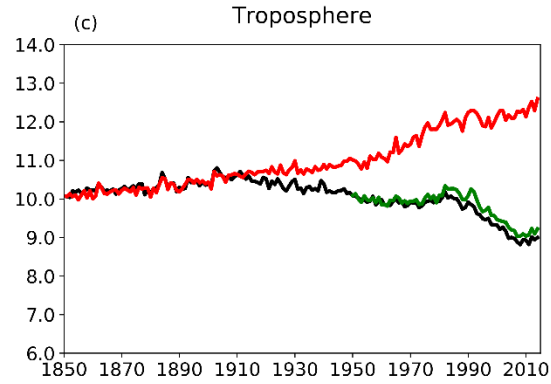
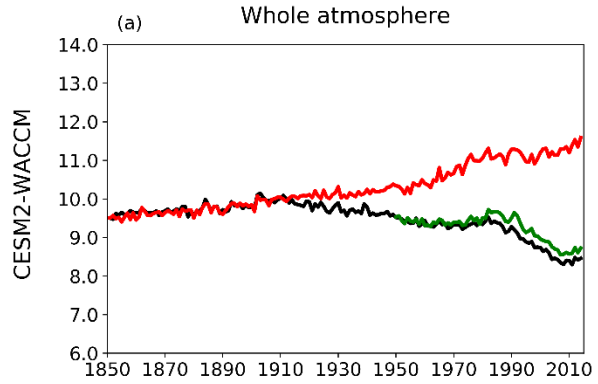
|088



089

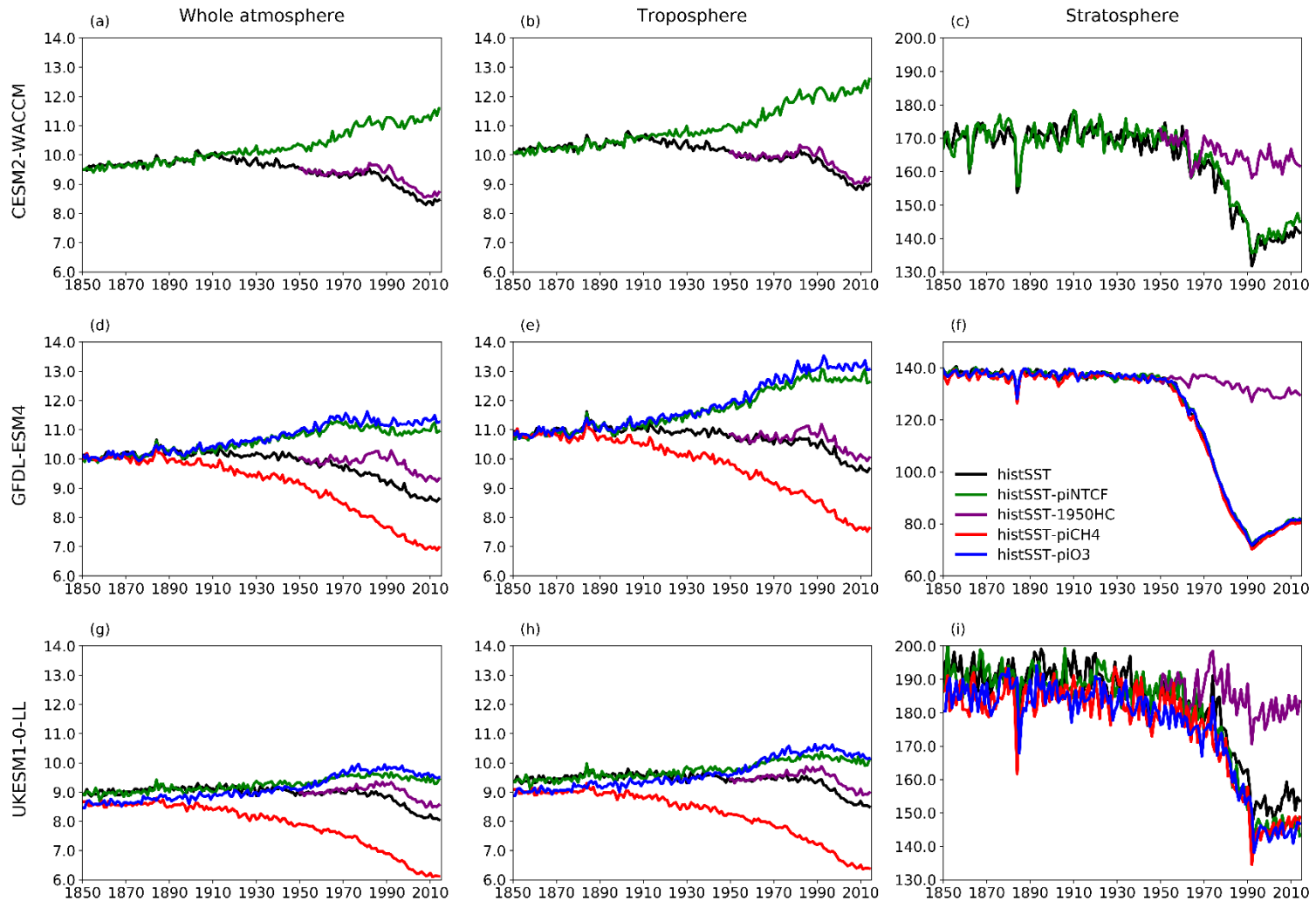
090 **Figure 5 Tropospheric OH anomaly (%) for sensitivity experiments from (a) CESM2-WACCM, (b) GFDL-ESM4 and**
 091 **(c) UKESM1. Note the values are expressed as a percentage anomaly relative to the 1850-1859 mean value in the**
 092 **histSST run in each model.**

093



096

Figure 6 The same format as Figure 5, but for

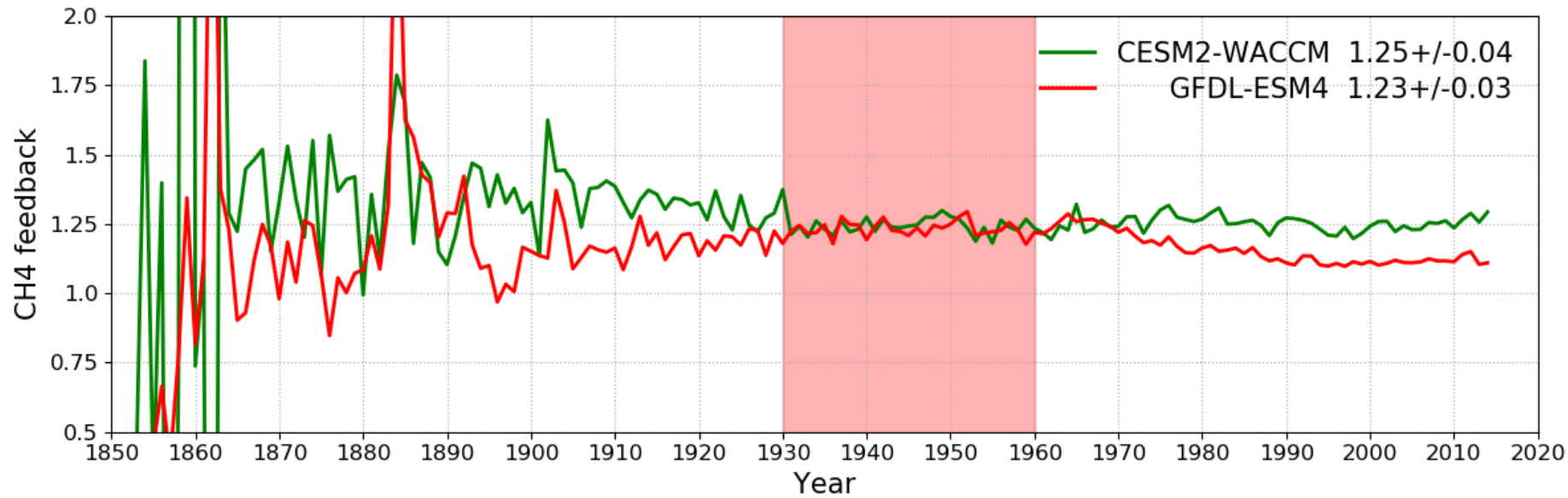


097

098 **Figure 7. Time evolution (1850-2014) of CH₄ lifetime (years) for (a-c) CESM2-WACCM; (d-f) GFDL-ESM4; and (g-i) UKESM1-0-LL, averaged over the whole atmosphere (left, d, g), the troposphere (middle, b, e, h), and the stratosphere (right, c, f, i). Colours refer to different model experiments, as indicated in panel (f). NB for UKESM1-0-LL, we used historical-piNTCF as histSST-piNTCF was not available.**

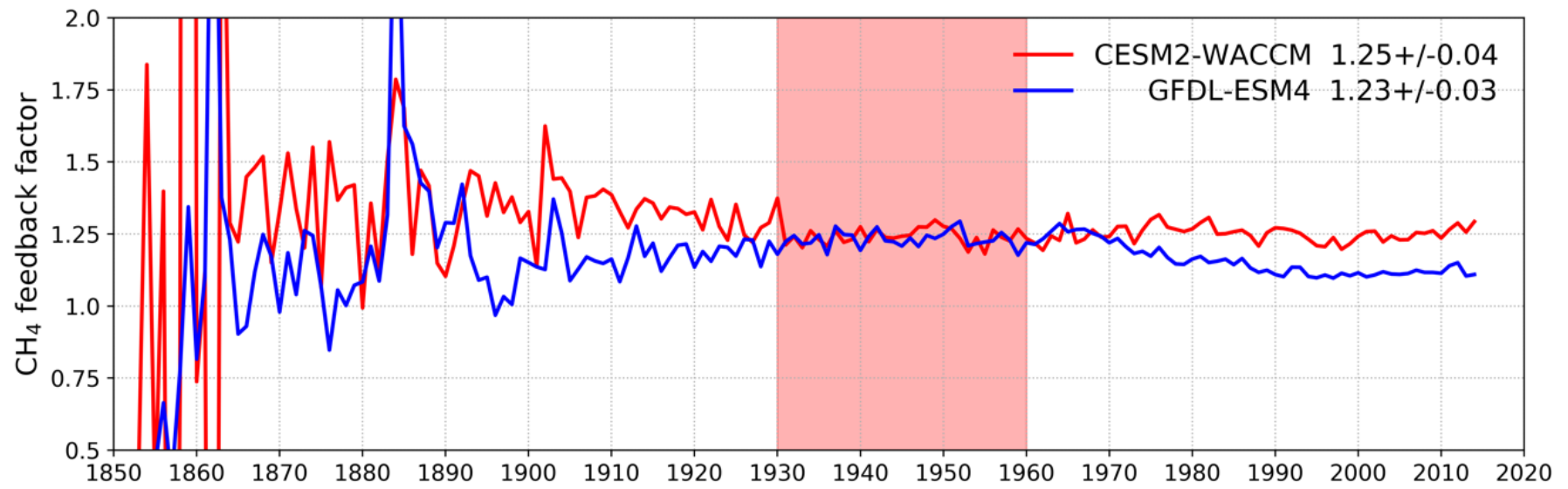
100

101



102

103



104

105

106 **Figure 78.** Calculated values for the methane-OH feedback factor (f) from the histSST_piNTCF experiments for ~~two models,~~ CESM2-WACCM and GFDL-ESM4. Mean and Standard
 107 Deviation values for 1930-1960 (shaded time period) are shown. ~~Calculation at other times is less reliable. See text for details.~~

108

1109
1110
1111

Table 1: Basic details of the AerChemMIP models analysed in this study. For more details see the model references.

Model	Resolution	Chemistry scheme	Interactive emissions	Interactive deposition	Reference
CESM2 (WACCM6)	0.9° lat 1.25° long 72 levels	Detailed troposphere/ stratosphere (228 species)	BVOC using MEGAN2.1 Lightning NOx	Yes	Gettelman et al. (2019); Emmons et al. (2019 2020)
UKESM1	1.875° long 1.25° lat 85 levels	Detailed stratosphere; 8 VOCs; 5 aerosols	BVOC Lightning NOx	Yes	Sellar et al., 2019; Archibald et al., 2019 2020; Mulcahy et al., 2019
GFDL	C96 (cubed sphere); nominally 1° 49 levels	ATMCHEM4.1 Interactive tropospheric/ stratospheric gas-phase/ aerosol chemistry.	BVOC Lightning NOx	No	Horowitz et al. submitted , 2020 ; Dunne et al., submitted 2020; Krasting et al. (2018)

1115

1120 Table 2: Number of ensemble members analysed from CMIP6 experiments in this study. All were transient 1850-2014 simulations, with evolving trace species emissions/GHG concentrations/mole fractions/land-surface. Baseline 'Historical' runs had freely evolving oceans, whilst 'histSST' runs were atmosphere only with prescribed (observed) SSTs and sea-ice. Sensitivity runs are based on histSST. The '-piNTCF' simulation held emissions of all NTCFs (aerosols and their precursors, and tropospheric ozone precursors) at PI levels. '-1950HC' held halocarbon concentrations/mole fractions at 1950 levels (essentially PI levels). '-piCH4' held methane concentrations/mole fractions at PI levels. '-piO3' held anthropogenic tropospheric ozone precursor emissions at PI levels.

1125

	Baseline runs		Sensitivity runs (based on histSST)*			
	historical	histSST	-piNTCF	-1950HC	-piCH4	-piO3
CESM2 (WACCM6) <u>WACCM</u>	3	1	1	1	NA	NA
UKESM1- <u>0-LL</u>	3	1	NA <u>1</u> *	1	1	1
GFDL- <u>ESM4</u>	1	1	1	1	1	1

1130

*UKESM1-0-LL sensitivity run for piNTCF is based on the historical (not histSST) run.

Table 3: Whole atmosphere methane chemical (not including soil sink) lifetimes (years). PI refers to 1850-1859 mean; PD refers to 2005-2014 mean. Uncertainties are ±1 Standard Deviation, based on the range of annual values.

	Historical		HistSST		piNTCF	1950HC	piCH4	piO3
	PI	PD	PI	PD	PD	PD	PD	PD
CESM2 (WACCM 6) WACCM	9.49 ±0.06	8.19 ±0.06	9.59 ±0.07	8.40 ±0.07	9.53 ±0.07	9.46 ±0.07	NA	NA
UKESM1- 0-LL	8.95 ±0.07	8.08 ±0.06	9.10 <u>8.96</u> ±0.08 0.0807	8.26 <u>13</u> ±0.05	NA <u>9.40</u> * ±0.08	8.85 <u>57</u> ±0.07 0.0708	6.48 <u>17</u> ±0.06	10.31 <u>9.57</u> ±0.07 0.0706
GFDL- ESM4	9.86 ±0.07	8.60 ±0.07	10.03 ±0.09	8.63 ±0.05	11.01 ±0.11	9.35 ±0.07	6.97 ±0.06	11.31 ±0.09

1135

1140 *UKESM1-0-LL methane lifetime for piNTCF is based on the historical (not histSST) run.

1145 Table 4: Equilibrium PD global mean methane ~~concentrations~~mole fractions (ppbv), inferred from PD methane lifetimes from the sensitivity experiments. Also shown are percentage changes compared to the observed PD value (1794 ppbv), or for the piCH4 case, the observed PI value (808 ppbv).

	piNTCF	1950HC	piCH4	piO3
CESM2	2082	2064	NA	NA
(WACCM6)	<u>2083</u>	<u>2065</u>		
<u>WACCM</u>	(+16%)	(+15%)		
<u>UKESM1-0-LL</u>	<u>2168</u>	<u>1917</u>	<u>505</u>	<u>2200</u>
	(+21%)	(+7%)	(-38%)	(+23%)
<u>GFDL-ESM4</u>	2377	1969	529	2451
	(+32) <u>2379</u>	(+10%)	<u>528</u>	<u>2454</u>
	(+33%)		(-35%)	(+37%)